Journal of Inorganic Biochemistry 264 (2025) 112808

Contents lists available at ScienceDirect

Journal of Inorganic Biochemistry

journal homepage: www.elsevier.com/locate/jinorgbio

Induction of ferroptosis of iridium(III) complexes localizing at the mitochondria and lysosome by photodynamic therapy

Yajie Niu [a], Shuanghui Tang [a], Jiongbang Li [a], Chunxia Huang [a], Yan Yang [b,*], Lin Zhou [a], Yunjun Liu [a,*], Xiandong Zeng [a,*]

[a] School of Pharmacy, Guangdong Pharmaceutical University, Guangzhou 510006, PR China
[b] Department of Pharmacy, The Affiliated Guangdong Second Provincial General Hospital of Jinan University, Guangzhou 510317, PR China

ARTICLE INFO

Keywords:
Iridium (III) metal complexes
Photosensitizer
Apoptosis
Ferroptosis
Immunogenic cell death

ABSTRACT

In this study, $[Ir(ppy)_2(DMHBT)](PF_6)$ (ppy = deprotonated 1-phenylpyridine, DMHBT = 10,12-dimethylpteridino[6,7-f][1,10]phenanthroline-11,13-(10,12H)-dione, 8a), $[Ir(bzq)_2(DMHBT)](PF_6)$ (bzq = deprotonated benzo[*h*]quinoline, 8b) and $[Ir(piq)_2(DMHBT)](PF_6)$ (piq = deprotonated 1-phenylisoquinoline, 8c) were synthesized and characterized by HRMS, ^{13}C NMR and ^{1}H NMR. In vitro cytotoxicity experiments showed that 8a, 8b, 8c show moderate cytotoxicity against B16 cells, while the cytotoxicity of the complexes 8a, 8b and 8c toward B16 cells was greatly improved upon light irradiation, which can be used as photosensitizers to exert anticancer efficacy in photodynamic therapy (PDT). After being taken up by cells, 8a, 8b, 8c were localized in the mitochondria, resulting in a large amount of Ca^{2+} in-flux, a burst release of ROS, a sustained opening of mitochondrial permeability transition pore, and a decrease of the mitochondrial membrane potential, which led to mitochondrial dysfunction and further activation of caspase 3 and Bcl-2 family proteins to induce apoptosis. Overloaded ROS reacted with polyunsaturated fatty acids on the cell membrane, and initiated lipid peroxidation, inhibited the x_c^--system-glutathione (GSH)-glutathione peroxidase 4 (GPX4) antioxidant defense system, and upregulated the expression of the damage-associated molecules, HMGB1, CRT, and HSP70. The presence of Fer-1 was effective on increasing the cell survival, which demonstrates that the complexes possess the potential to induce ferroptosis and immunogenic cell death. In addition, 8a, 8b and 8c induced autophagy by inhibiting the AKT/PI3K/mTOR signaling pathway, downregulating p62 and promoting Beclin-1 expression upon light irradiation.

Abbreviations: 8a, $[Ir(ppy)_2(DMHBT)](PF_6)$; 8b, $[Ir(bzq)_2(DMHBT)](PF_6)$; 8c, $[Ir(piq)_2(DMHBT)](PF_6)$ 8a(light), 8b(light) and 8c(light) stands for the treatment of the cells with complexes 8a, 8b and 8c for 4 h, then irradiation for 30 min (LED lamp, 460 nm, 7.03 J/cm^2).; A549, human lung carcinoma; B16, mouse melanoma cells; AKT, protein kinase B; Bak, Bcl-2, homologous antagonist/killer; Bax, Bcl-2 associated x protein; Bcl-2, B-cell lymphoma-2; Beclin1, recombinant Beclin 1; bzq, deprotonated benzo[*h*]quinoline; C11-BODIPY$^{581/591}$, 4,4-difluoro-5-(4-phenyl-1,3-butadienyl)-4-bromo-3a,4a-diaza-s-indene-3-undecanedioic acid; calcein AM, calcein acetoxymethyl ester; caspase 3, cysteinyl aspartate specific proteinase 3; CRT, calreticulin protein; DAMPs, damage-associated molecular patterns; DAPI, 4′,6-diamidino-2-phenylindole; DHR123, dihydrorhodamine 123; DCFH-DA, 2′,7′-dichlorodihydro-fluorescein diacetate; DHE, dihydroethidium; DMHBT, 10,12-dimethylpteridino[6,7-f][1,10]phenanthroline-11,13-(10,12H)-dione; DMSO, dimethylsulfoxide; DPBF, 1,3-diphenylisobenzofuran; Fer-1, ferrostatin-1; GPX4, glutathione peroxidase 4; GSH, glutathione; HMGB1, high mobility group box-1; HOMO, highest occupied molecular orbital; HPF, hydroxyphenyl fluorescein; HPLC, high performance liquid chromatography; HRMS, high resolution mass spectrometry; HSP70, heat shock protein 70; IC_{50}, half-maximum inhibitory concentration; ICD, immunogenic cell death; JC-1, 5,5′,6,6′-tetrachloro-1,1′,3,3′-tetraethylbenzenecarboxamidinylcarbocyanine iodide; LC3, autophagy marker light chain 3; LDH, lactate dehydrogenase; LO2, human normal hepatocytes; logP, lipid-water partition coefficient; LUMO, lowest unoccupied molecular orbital; MDA, malondialdehyde; MDIP, 2-(7-methoxybenzo[d][1,3]dioxol-5-yl)-1H-imidazo[4,5-f][1,10]phenanthroline; m-TOR, mammalian target of rapamycin; MTT, 3-(4,5-dimethylthiazole-2-yl)-diphenyltetrazolium bromide; MMP, mitochondrial membrane potential; MPTP, mitochondrial membrane permeability transition pore; NMR, nuclear magnetic resonance; p62, polyubiquitin-binding protein; PARP, poly ADP-ribose polymerase; PBS, phosphate buffer saline; PDT, photodynamic therapy; PI3K, phosphatidylinositol 3-kinase; piq, deprotonated 1-phenylisoquinoline; p-mTOR, phosphorylated mammalian target of rapamycin; PPD, pteridino[6,7-f][1,10]phenanthroline-11,13-diamine; ppy, deprotonated 1-phenylpyridine; PVDF, polyvinylidene difluoride; ROS, reactive oxygen species..

* Corresponding authors.
E-mail addresses: yany@gd2h.org.cn (Y. Yang), lyjche@gdpu.edu.cn (Y. Liu), zengxiandong@gdpu.edu.cn (X. Zeng).

https://doi.org/10.1016/j.jinorgbio.2024.112808
Received 14 October 2024; Received in revised form 12 November 2024; Accepted 6 December 2024
Available online 9 December 2024

1. Introduction

Melanoma is a highly metastatic tumor that can spread rapidly throughout the body, making it difficult for radiotherapy and chemotherapy to effectively counteract the development of highly diffuse metastases [1,2]. Photodynamic therapy (PDT) is a cancer treatment modality based on the interaction between photosensitizers, light, and molecular oxygen, and the use of photoexcitation of photosensitizers to produce cytotoxic oxygen-related substances that promote tumor cell death through necrosis or apoptosis [3,4]. Generally, the photosensitizers need a long triplet excited state lifetime to prompt electron transfer to produce oxygen radicals (type I pathway) or energy transfer to generate singlet oxygen ($^1O_2$, type II pathway) [5–7]. In recent years, photodynamic therapy (PDT) has been indicated as an effective means to improve melanoma treatment [8,9]. It has been shown that PDT can achieve long-term tumor control through immune induction of tumor cells and enhancement of the ferroptosis pathway, respectively [9,10]. Liu et al. found that $[Ir(bzq)_2(PPD)](PF_6)$ (PPD = pteridino[6,7-f][1,10] phenanthroline-11,13-diamine) shows no cytotoxic activity ($IC_{50} > 100$ μM), upon light irradiation, the IC_{50} value is 18.0 ± 1.6 μM, while the complex was entrapped into the liposome and exhibits very high cytotoxic efficiency ($IC_{50} = 4.1 \pm 0.2$ μM) [11]. Chao et al. reported that the functionalized Ir(III) complexes selectively localize at the mitochondria and produce $^1O_2$ and $O_2^{\bullet-}$ upon two-photon irradiation to efficiently prevent the tumor growth [12]. Additionally, after irradiation, $[Ir(C^{\wedge}N)_2(dppz)]^+$ caused leakage of lysosomal content into the cytoplasm and induced oncosis-like cell death in HeLa cells [13]. Most these compounds are type II photosensitizers, namely, the photosensitizers transfer its energy to molecular oxygen ($^3O_2$), resulting in population of singlet oxygen ($^1O_2$), $^1O_2$ is reactive species able to kill cells [14]. As a photosensitizer in photodynamic therapy (PDT), we also uncovered that the iridium(III) complexes can transfer $^3O_2$ into $^1O_2$ to promote cancer cell apoptosis in our lab [15–17].

To gain more insight into the anticancer activity, in this article, we designed and synthesized $[Ir(ppy)_2(DMHBT)](PF_6)$ (ppy: 1-phenylpyridine, DMHBT: 10,12-dimethylpteridino[6,7-f][1,10]phenanthroline-11,13-(10,12H)-dione, 8a), $[Ir(bzq)_2(DMHBT)](PF_6)$ (bzq: benzo[*h*] quinoline, 8b) and $[Ir(piq)_2(DMHBT)](PF_6)$ (piq: 1-phenylisoquinoline, 8c). 8a and 8b display moderate or low cytotoxicity toward B16 and A549 cells. To improve the anticancer efficiency, the co-incubation of

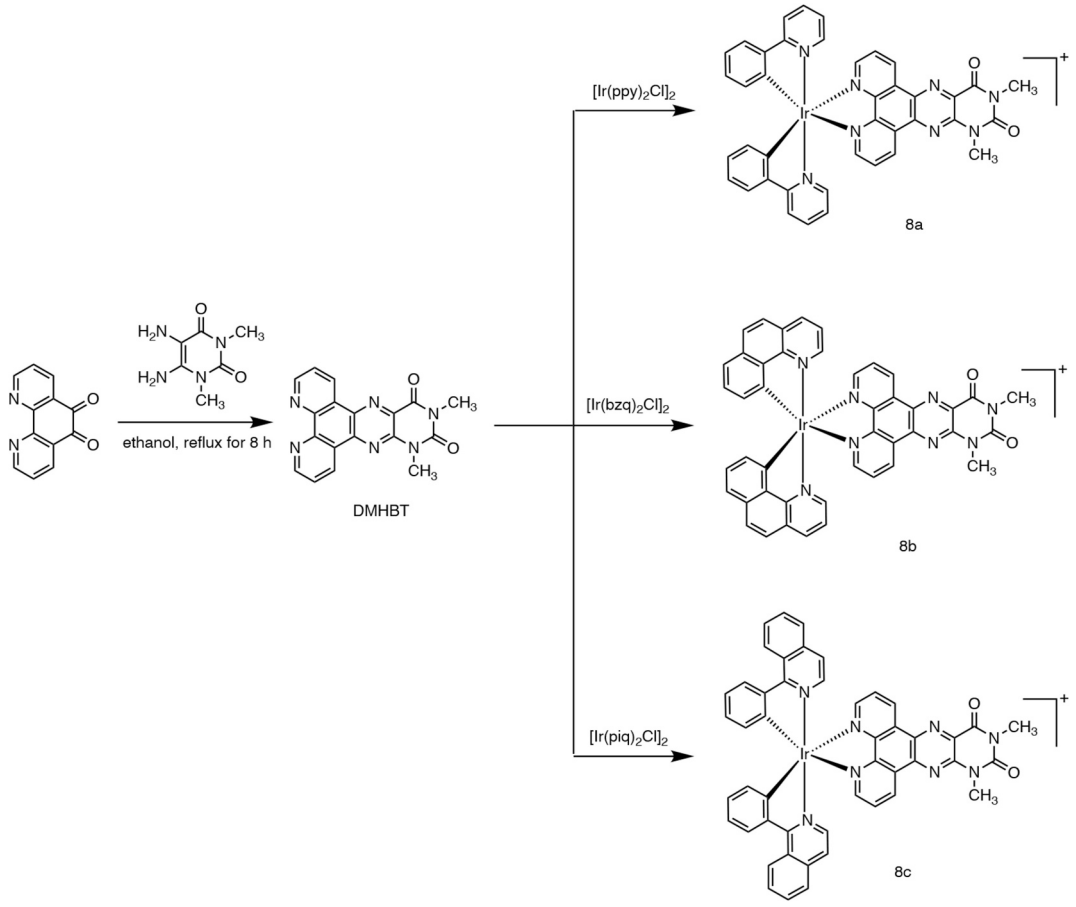

Scheme 1. Synthetic route of DMHBT, 8a, 8b and 8c.

Table 1
IC_{50} (μM) values of 8a, 8b and 8c toward the selected cancer cells for 48 h.

complex	B16		SI	A549		SI	LO2	
	IC_{50dark}	$IC_{50light}$		IC_{50dark}	$IC_{50light}$		IC_{50dark}	$IC_{50light}$
8a	25.2 ± 2.3	8.2 ± 0.2		49.0 ± 8.9	37.6 ± 2.7		> 100	> 100
8b	11.4 ± 1.2	6.5 ± 0.2	5.3	37.6 ± 4.6	16.8 ± 3.1	2.0	47.1 ± 2.8	34.2 ± 5.4
8c	1.6 ± 0.1	1.1 ± 0.1	5.4	1.4 ± 0.2	1.0 ± 0.1	5.9	13.3 ± 1.9	5.9 ± 0.9
cisplatin	18.3 ± 1.4	—		6.3 ± 0.5	—		18.2 ± 2.2	—

Selectivity Index (SI): IC_{50} value of LO2 versus cancer cells upon light irradiation.

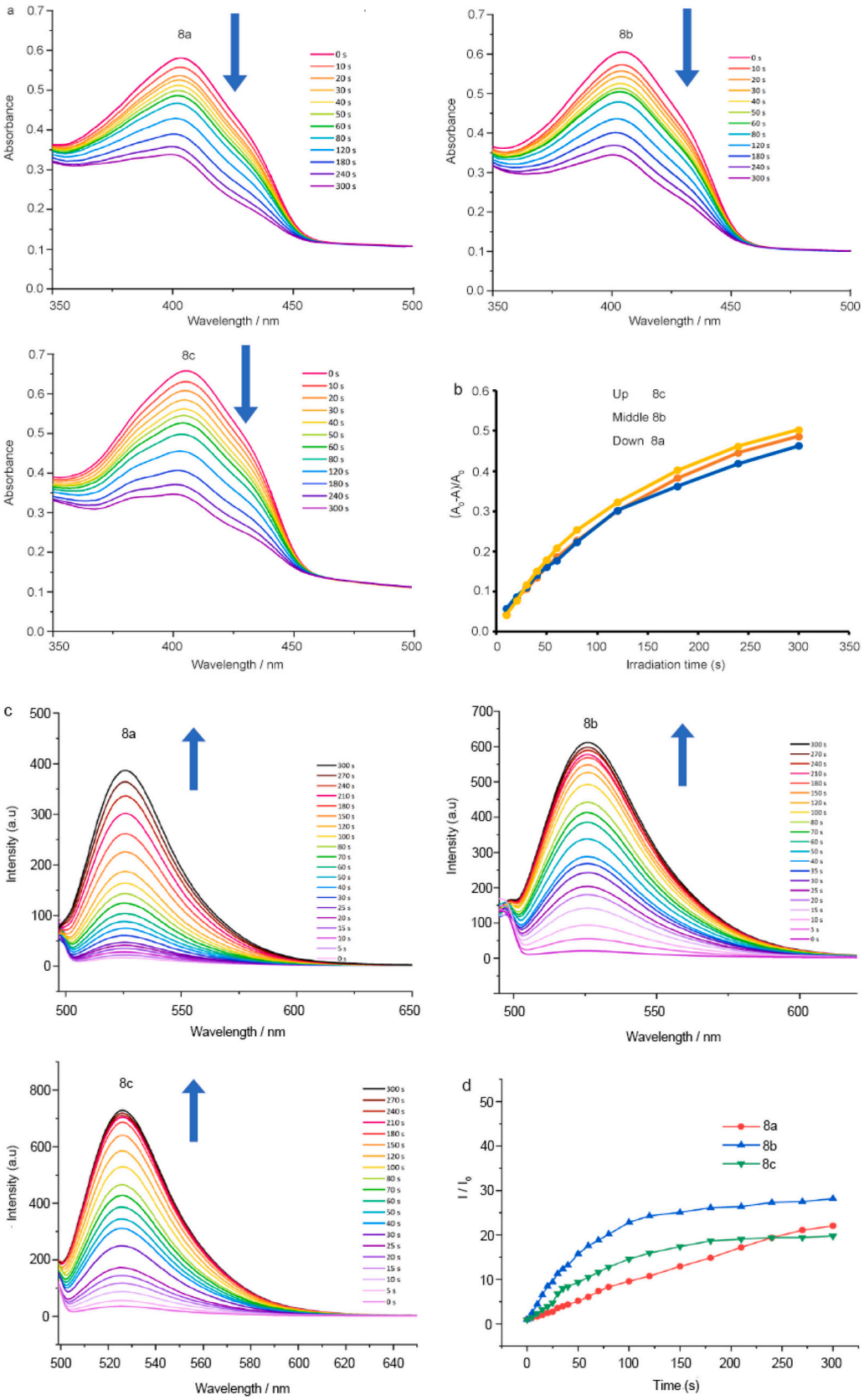

Fig. 1. (a and b) The change in the absorbance of DPBF at 412 nm during 3 min light irradiation, [DPBF] = 20 μM, [Ir complexes] = 10 μM, (c and d) superoxide anion assay using DHR123 as a probe, [DHR123] = 10 μM, [Ir complexes] = 10 μM, (e and f) Energy gap between LUMO and HOMO orbitals or between S_1 and T_1.

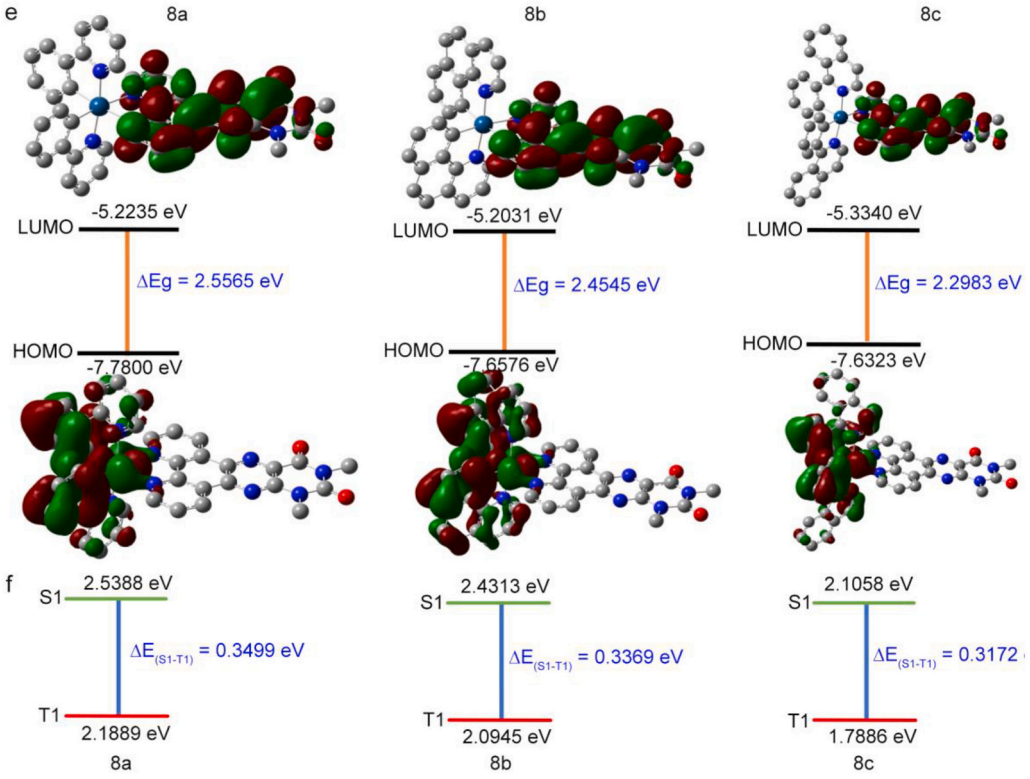

Fig. 1. (*continued*).

cancer cells with 8a, 8b and 8c for 4 h, the cells were irradiated for 30 min (LED lamp, 460 nm, 7.03 J/cm^2), we unexpectedly found that the anticancer efficiency of 8a [8a(light)], 8b [(8b(light)] and 8c [(8c (light)] on B16 cells was greatly enhanced. Thereafter, we explored the anticancer effect and mechanism through apoptosis, ROS, mitochondrial membrane potential, autophagy and so on. The results demonstrate that 8a(light), 8b(light) and 8c(light) trigger cell demise by apoptosis, autophagy and ferroptosis.

2. Experimental

2.1. Synthesis and characterization

2.1.1. Synthesis of $[Ir(ppy)_2(DMHBT)]PF_6$ (8a)

Under argon, DMHBT (0.17 g, 0.5 mmol) [18] and Cis-$[Ir(ppy)_2Cl]_2$ (0.27 g, 0.25 mmo1) [19] were reacted in 15 mL of methanol and 30 mL dichloromethane at a constant temperature of 40 °C for 6 h, then 1.0 g of ammonium hexafluorophosphate was added after the solution was cooled to room temperature and continuously stirred for 1.5 h. After removing the solvent in the filtrate, a yellow-brown solid was gained. Neutral alumina column chromatography was used to purify the crude product (CH_2Cl_2 and CH_3COCH_3 (5:1, *v*/v) as eluent), the bright yellow band was gathered, the solvent was removed to give a bright yellow product. Yield: 80 %. HRMS (CH_3CN, Fig. S1, SI): Calcd for $C_{40}H_{28}IrN_8O_2PF_6$: $m/z = 845.1964$ ($[M\text{-}PF_6]^+$), found: $m/z = 845.2012$. ^{1}H NMR (DMSO-d_6, 500 MHz, Fig. S2, SI): δ 9.73 (d, 1H, $J = 8.0$ Hz), 9.49 (d, 1H, $J = 8.0$ Hz), 8.34 (d, 1H, $J = 4.5$ Hz), 8.29 (d, 3H, $J = 7$ Hz), 8.23–8.16 (m, 2H), 7.97 (d, 2H, $J = 8.0$ Hz), 7.90 (t, 2H, $J = 7.5$ Hz), 7.61 (t, 2H, $J = 5.5$ Hz), 7.08 (t, 2H, $J = 7.5$ Hz), 7.04–7.00 (m, 2H), 6.97 (t, 2H, $J = 7.0$ Hz), 6.28 (d, 2H, $J = 7.5$ Hz), 3.86 (s, 3H), 3.47 (s, 3H). ^{13}C NMR (DMSO-d_6, 125 MHz, Fig. S3, SI): 178.30, 172.51, 167.25, 162.80, 159.55, 153.03, 151.70, 151.08, 150.00, 148.16, 147.95, 144.51, 141.14, 139.30, 136.55, 134.81, 134.61, 131.66, 130.78, 130.26, 129.54, 129.09, 128.80, 125.60, 124.33, 122.99, 36.26, 31.25.

2.1.2. Synthesis of $[Ir(bzq)_2(DMHBT)]PF_6$ (8b)

The synthesis of 8b was similar to 8a, with the substitution of cis-$[Ir(bzq)_2Cl]_2$ (0.25 mmol, 0.30 g) [19] for cis-$[Ir(ppy)_2Cl]_2$. Yield: 87 %. HRMS (CH_3CN, Fig. S4, SI): Calcd for $C_{44}H_{28}IrN_8O_2PF_6$: $m/z = 893.2874$ ($[M\text{-}PF_6]^+$), found: $m/z = 893.2935$. ^{1}H NMR (DMSO-d_6, 500 MHz, Fig. S5, SI): δ 9.72 (d, 1H, $J = 8.0$ Hz), 9.47 (d, 1H, $J = 8.0$ Hz), 8.54 (d, 2H, $J = 8.0$ Hz), 8.32 (dd, 1H, $J = 1.0$, $J = 5.0$ Hz), 8.27 (dd, 1H, $J = 1.0$, $J = 5.0$ Hz), 8.12–8.06 (m, 4H), 7.99 (d, 2H, $J = 8.0$ Hz), 7.89 (d, 2H, $J = 8.5$ Hz), 7.59 (d, 2H, $J = 8.0$ Hz), 7.49–7.45 (m, 2H), 7.23 (t, 2H, $J = 7.5$ Hz), 6.30 (d, 2H, $J = 7.5$ Hz), 3.86 (s, 3H), 3.47 (s, 3H). ^{13}C NMR (DMSO-d_6, 125 MHz, Fig. S6, SI): 172.51, 162.79, 159.57, 156.72, 153.57, 152.24, 151.09, 150.41, 149.79, 148.40, 148.17, 146.79, 141.19, 140.77, 138.10, 136.56, 134.85, 134.64, 134.23, 130.80, 130.25, 130.22, 129.96, 129.53, 129.06, 128.98, 128.77, 127.17, 124.71, 123.23, 123.19, 120.99, 36.25, 31.24.

2.1.3. Synthesis of $[Ir(piq)_2(DMHBT)]PF_6$ (8c)

The synthesis and purification of 8c was the same as 8a, with the substitution of cis-$[Ir(piq)_2Cl]_2$ (0.25 mmol, 0.32 g) [19] for cis-$[Ir(ppy)_2Cl]_2$. Yield: 78 %. HRMS (CH_3CN, Fig. S7, SI): Calcd. for $C_{48}H_{32}IrN_8O_2PF_6$: $m/z = 945.2280$ ($[M\text{-}PF_6]^+$), found: $m/z = 945.2111$. ^{1}H NMR (DMSO-d_6, 500 MHz, Fig. S8, SI): δ 9.75 (t, 1H, $J = 5.0$ Hz), 9.52–9.50 (m, 1H), 9.02 (d, 2H, $J = 9.0$ Hz), 8.41 (d, 2H, $J = 8.0$ Hz), 8.20 (d, 2H, $J = 4.5$ Hz), 8.15 (d, 2H, $J = 4.0$ Hz), 8.08–8.03 (m, 2H), 7.91–7.87 (m, 4H), 7.52–7.45 (m, 4H), 7.19 (t, 2H, $J = 7.5$ Hz), 7.00–6.97 (m, 2H), 6.27 (t, 2H, $J = 6.5$ Hz), 3.86 (s, 3H), 3.48 (s, 3H). ^{13}C NMR (DMSO-d_6, 125 MHz, Fig. S9, SI): 168.26, 162.78, 159.54, 153.38, 153.35, 153.00, 151.66, 151.09, 149.80, 148.20, 147.79, 145.84, 141.66, 141.61, 141.19, 137.05, 136.63, 134.86, 134.72, 132.57, 132.12, 132.08, 131.16, 131.08, 130.83, 130.36, 129.87, 129.63, 129.11, 128.82, 128.15, 126.94, 126.00, 122.98, 122.63, 36.26, 31.24.

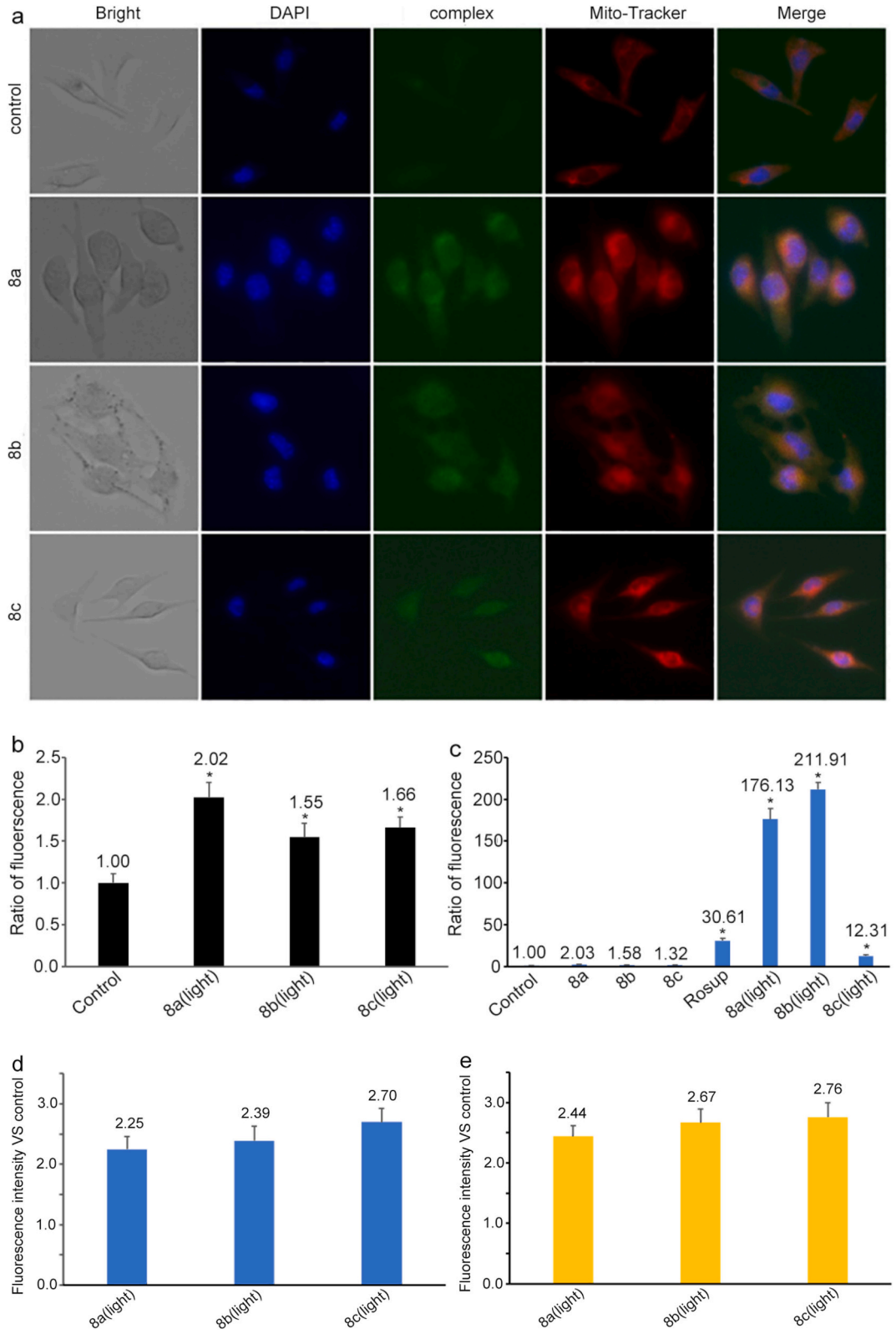

Fig. 2. (a) The co-location of 8a, 8b and 8c in the mitochondria after an exposure of B16 cells to IC_{50} concentration for 4 h. (b) Intracellular Ca^{2+} content, (c) ROS levels, (d) superoxide anion assay using DHE as a probe upon light irradiation, DHE fluorescence intensity, [DHE] = 5 μM, [Ir complexes] = 2 × IC_{50} μM, (e) hydroxyl free radical assay with HPF as a probe upon irradiation, HPF fluorescence intensity, [HPF] = 10 μM, [Ir complexes] = 2 x IC_{50} μM, (f) MPTP assay, (g) change of the mitochondrial membrane potential and (h) the ratio of red/green in B16 cells treated with IC_{50} concentration of 8a(light), 8b(light) and 8c(light) for 24 h. (For interpretation of the references to colour in this figure legend, the reader is referred to the web version of this article.)

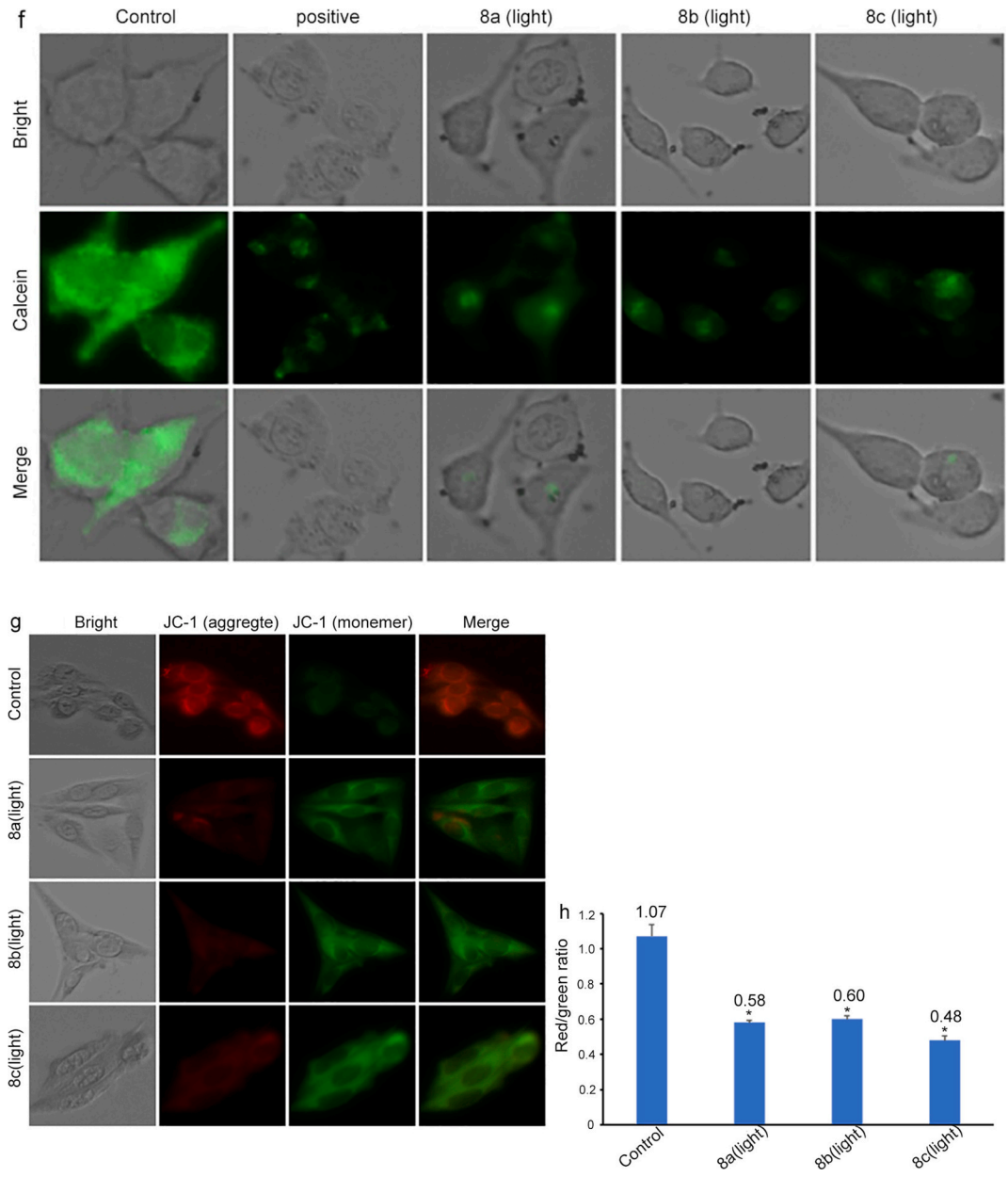

Fig. 2. (*continued*).

2.2. Determination of purity

The purity of 8a, 8b and 8c was determined at 25 °C via HPLC. The mobile phases A and B were H_2O and CH_3OH with a flow rate of 3 mL/min. The purity of 8a, 8b and 8c was determined by different elution programs of H_2O:CH_3OH of 7:93 for 8a, 5:95 for 8b, and 10:90 for 8c, with a detected wavelength of 210 nm.

2.3. In vitro toxicity assay

The in vitro cytotoxicity of 8a, 8b and 8c on cancer cells was explored using 3-(4,5-dimethylthiazole-2-yl)-diphenyltetrazolium bromide (MTT) [20]. The cells were homogeneously incubated in 96-well plates (2.5 x 10^5 cells per well) for 24 h and treated with a series of concentration gradient of 8a, 8b and 8c (1.56, 3.125, 6.25, 12.5, 25.0, 50.0, 100 μM) for 4 h, then the cells were irradiated for 30 min (LED lamp, 460 nm, 7.03 J/cm^2) and continuously cultured for 24 h. The culture medium was discarded, and the cells were treated with MTT (9:1, *v*/v), after 4 h, discarding the culture medium and 100 μL of DMSO was used to dissolve residual MTT, recording the absorbance at 490 nm.

2.4. Intracellular lipid peroxidation

C11-BODIPY$^{581/591}$ is a fluoroboron fluorescent derivative with good photostability and low fluorescence artifacts for further determination of intracellular lipid peroxidation. In the qualitative experiments, B16 cells (4×10^5 per well) were inoculated into 6-well plates for 24 h and exposed to 8a (8.2 μM), 8b (6.5 μM) and 8c (1.1 μM) for 4 h and irradiated for 30 min (LED lamp, 460 nm, 7.03 J/cm^2), and progressively cultured for 24 h. The cells were washed and dyed with C11-BODIPY$^{581/591}$ (2.5 μM) for 30 min at 37 °C, ultimately, the cells were subsequently observed under a microscope.

2.5. Ferrostatin-1 (Fer-1) assay

Cultured in 96-well plates (1×10^4 cells per well) for 24 h, B16 cells

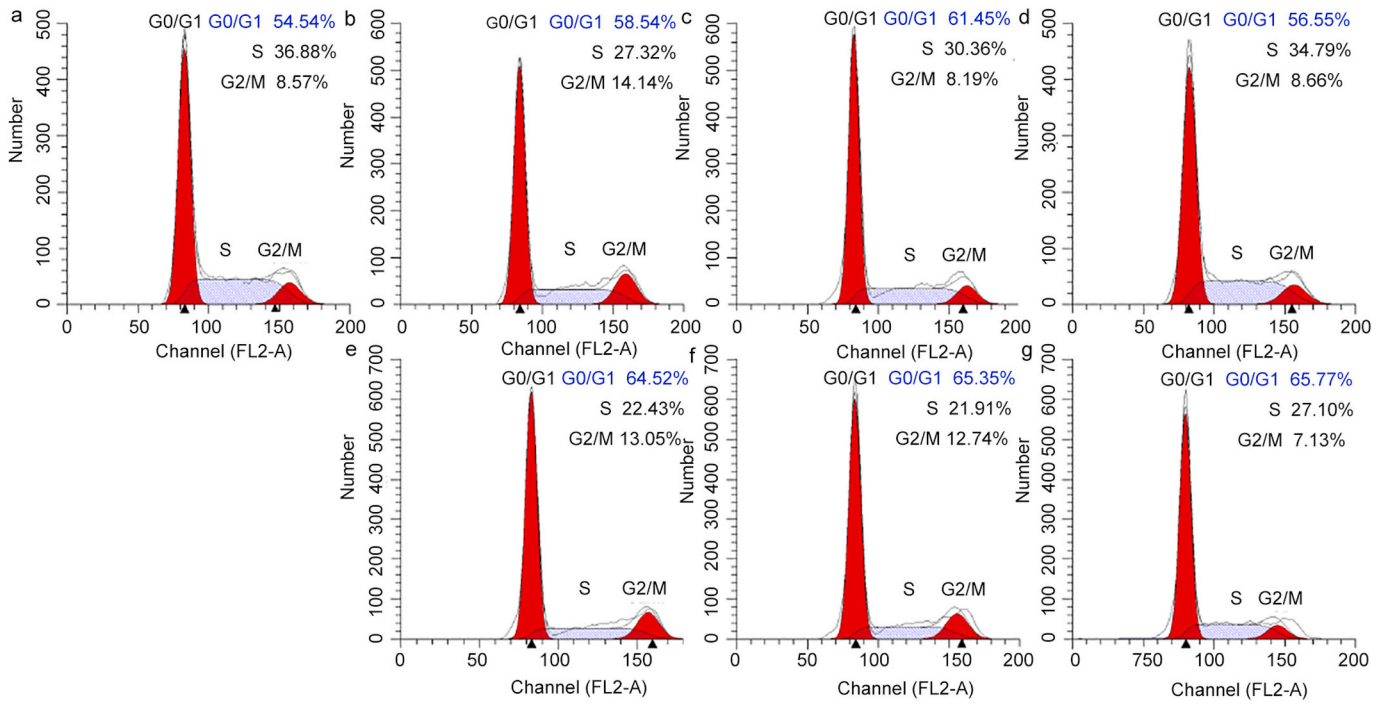

Fig. 3. Cell cycle distribution was detected after an exposure of B16 cells (a) to IC_{50} concentration of 8a (b), 8b (c), 8c (d), 8a(light, e), 8b(light, f) and 8c(light, g) for 24 h.

were treated via the following eight groups: (I) blank group, (II) blank group + Fer-1, (III) 8a(light), (IV) 8a(light) + Fer-1, (V) 8b(light), (VI) 8b(light) + Fer-1, (VII) 8c(light), and (VIII) 8c(light) + Fer-1 for 4 h, the cells were irradiated for 30 min (LED lamp, 460 nm, 7.03 J/cm^2), and continuously cultured for 24 h, then MTT was added into the cells and the cell viability was measured.

2.6. Western blot analysis

Equal amounts of protein samples of the same concentration were loaded into each lane of a sodium dodecyl sulfate-polyacrylamide gel and electrophoresed for 3 h (50 V, 400 mA). Gel proteins were transferred semi-dry onto PVDF membranes in an all-purpose protein transfer system for 20 min, and the PVDF membranes loaded with protein bands were closed with 0.5 % skimmed milk for 1 h. The membrane was incubated with the primary antibody at 4 °C in a refrigerator overnight. Next day, the primary antibody was removed, the cells were incubated with the second antibody for 1 h. Finally, the protein bands were observed in FluorChem E.

2.7. Data analysis

All data were expressed using mean ± SD. And *t*-test was used to evaluate the statistical significance. $^*P < 0.05$ indicates a significant difference.

3. Results and discussion

3.1. Synthesis and characterization

The ligand DMHBT was prepared with 1,10-phenanthroline-5,6-dione and 5,6-diamino-1,3-dimethyluridine in ethanol and refluxed for 8 h. The corresponding iridium(III) complexes 8a, 8b and 8c were obtained by the reaction of DMHBT with $[Ir(ppy)_2Cl]_2$, $[Ir(bzq)_2Cl]_2$ and $[Ir(piq)_2Cl]_2$ in CH_3OH/CH_2Cl_2 (Scheme 1). In the ^{1}H NMR spectra, 3.86 (s,3H) and 3.47 (s, 3H) for 8a and 8b, 3.86 (s, 3H) and 3.48 (s, 3H) for 8c are attributed to the protons in the two methyl groups (-CH_3). 178.30 ppm for 8a, 172.51 ppm for 8b, 168.26 ppm for 8c are assigned to the carboxyl groups, while 36.26 and 31.25 ppm for 8a, 36.25 and 31.24 ppm for 8b and 36.26 and 31.24 ppm for 8c are allocated to the two carbon atoms in the two -CH_3 groups.

8a, 8b and 8c display two or three peaks, 268 nm (ε = 48,900), 366 nm (ε = 20,500) and 400 nm (ε = 12,500) for 8a, 262 nm (ε = 32,396), 359 nm (ε = 16,957) and 401 nm (ε = 12,504) for 8b, 289 nm (ε = 31,066) and 384 nm (ε = 18,705) for 8c, respectively (Fig. S10, SI). 8a, 8b and 8c emit weak green fluorescence, with a maximum locating at 604, 603 and 614 nm (Fig. S11, SI).

The stability of 8a, 8b and 8c was measured and found that the peak shapes during 72 h have no change, indicating that 8a, 8b and 8c are stable in PBS solution (Fig. S10, SI).

The purity of 8a, 8b and 8c was examined by HPLC (Fig. S12, SI), only one main peak was found during 30 min, indicating that 8a, 8b and 8c are pure (purity >95 %).

3.2. Lipid-water partition coefficient (logP) and in vitro cytotoxicity studies

Lipid-water partition coefficient (logP) is used to determine the concentration of a compound in the lipid phase and the aqueous phase according to the literature [21]. The logP values are −0.19, 0.32 and −0.49 for 8a, 8b and 8c, suggesting that 8a, 8b and 8c can enter cells. Based on the principle that succinate dehydrogenase in the mitochondria of living cells can reduce exogenous 3-(4,5-dimethylthiazole-2-yl)-diphenyltetrazolium bromide (MTT) to blue-violet crystalline formazan, whereas dead cells do not have such a function, we have used the MTT colorimetric assay to examine the cytotoxicity of 8a, 8b, and 8c on B16 and A549 cancer cells. As listed in the Table 1, 8a and 8b showed moderate or low cytotoxic effects on B16 and A549 in the dark, while 8c showed strong anti-tumor activity on B16 and A549 cells. To enhance anticancer activity, after the treatment of cancer cells with the complexes for 4 h and irradiation (LED lamp, 460 nm, 7.03 J/cm^2) for 30 min, the anticancer efficiency was greatly enhanced, particularly, 8a, 8b and 8c show high anticancer efficiency on B16 cells with low IC_{50} values of 8.2 ± 0.2, 6.5 ± 0.2 and 1.1 ± 0.1 μM, but these complexes show low

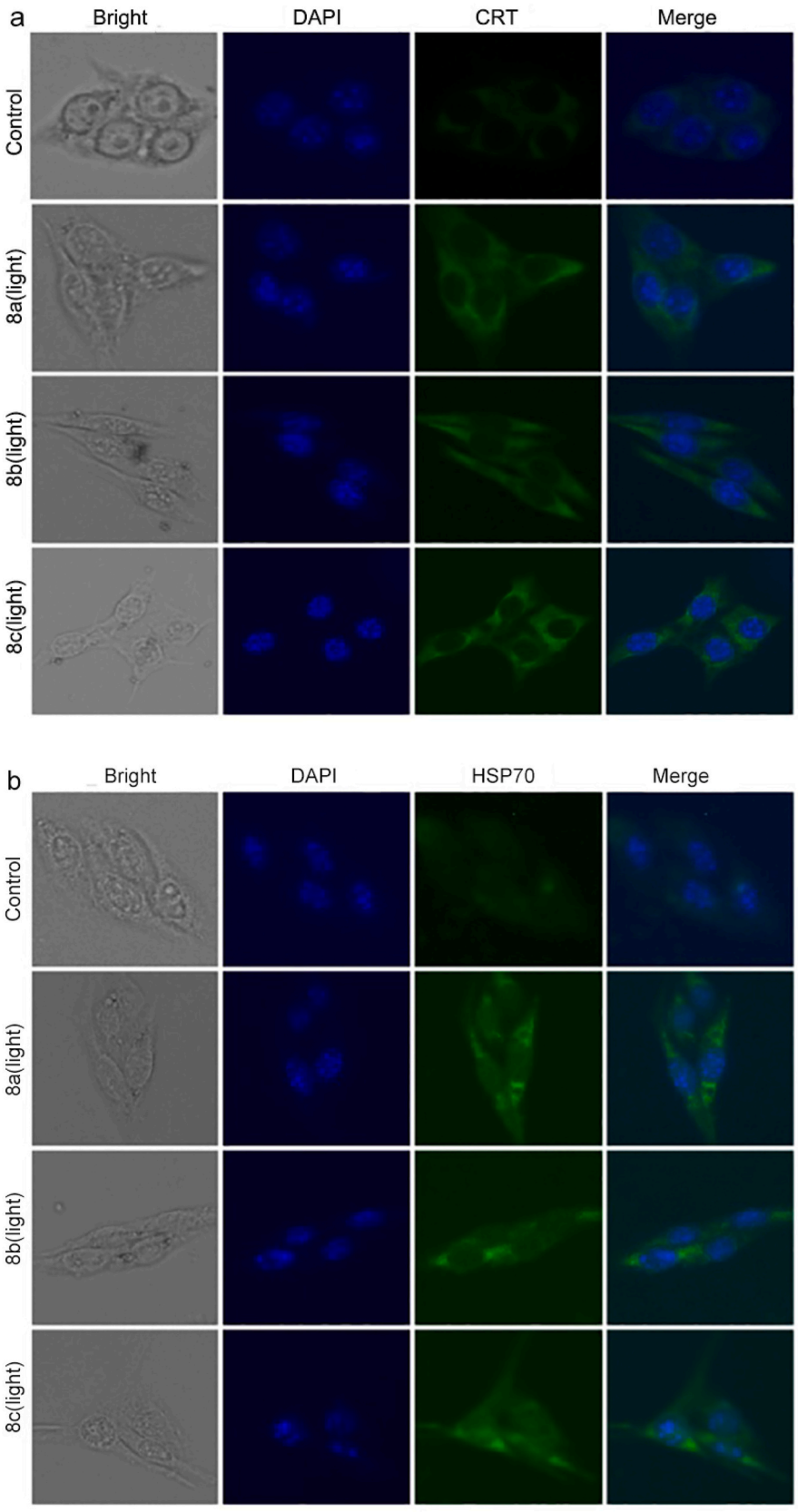

Fig. 4. The intracellular CRT (a), HSP70 (b) and HMGB1 (c) assays in B16 cells treated with IC_{50} concentrations of 8a(light), 8b(light) and 8c(light) for 24 h.

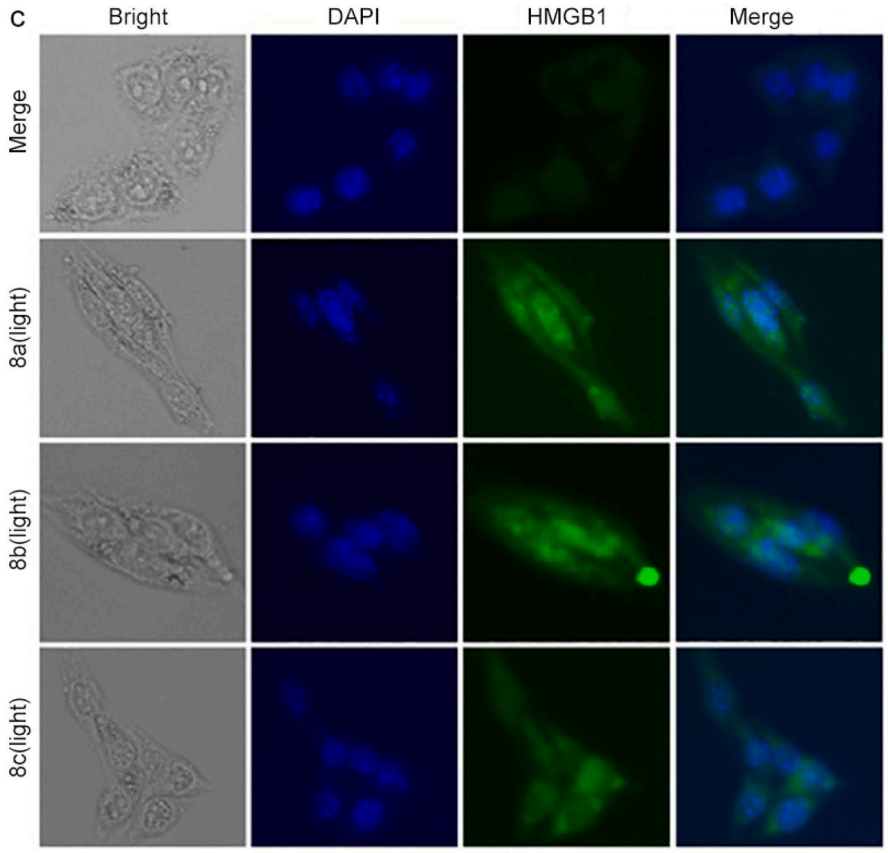

Fig. 4. (*continued*).

selectivity index (SI) values (Table 1). The cytotoxic activity of 8a(light), 8b(light) and 8c(light) is higher than cisplatin, but lower than [Ir(ppy)$_2$(MDIP)](PF$_6$) (IC_{50} = 0.7 ± 0.3 μM) [16] and organo-iridium–albumin bioconjugate Ir(III) complex Ir-HSA (human serum albumin) (IC_{50} = 1.1 ± 0.3 μM) [22].

Comparing the cytotoxicity of 8a, 8b and 8c on B16 and A549 cells, B16 cells were selected for the subsequent series of experiments.

Photodynamic therapy (PDT) has been widely applied in cancer treatment due to its unique spatial selectivity and low toxicity, and it has been reported that singlet oxygen ($^1O_2$) is the key to the death. The photosensitizer is irradiated by a light source in the ground state to become an excited state, and in the excited state photosensitizer transfers energy to the ground state oxygen to generate $^1O_2$, which is capable of damaging cells and causing cell death [23–27]. Light irradiation enhances cytotoxic activity of 8a, 8b and 8c on B16 and A549 cells, this is closely to the generation of singlet oxygen ($^1O_2$) or superoxide anion ($O_2^{\bullet-}$). Firstly, we investigated $^1O_2$ and quantum yield Φ. 1,3-Diphenylisobenzofuran (DPBF) is a singlet oxygen capture agent that can indirectly detect $^1O_2$. As shown in the Fig. 1a and b, during 5 min, a decrease of 48.7 % for 8a, 46.2 % for 8b, 50.3 % for 8c was discovered in the absorbance of DPBF at 417 nm. Owing to the moderate change in the absorbance of DPBF, which indicated that 8a, 8b and 8c show a moderate ability to generation of $^1O_2$. While in our previous work [28], we discovered that the iridium(III) complex [Ir(piq)$_2$(DBDIP)](PF$_6$) (DBDIP = 2-(2,3-dihydrobenzo[b][1,4]dioxin-6-yl)-1H-imidazo[4,5-f][1,10] phenanthroline) containing dioxane ring shows very significant phototoxicity, before and after illumination, the change in the absorbance of DPBF reached 95.29 %, the IC_{50} values change from >100 to 1.7 ± 0.1 μM and > 100 to 0.31 ± 0.1 μM toward BEL-7402 and A549 cells, respectively. Hence, the photocytotoxicity of 8a, 8b and 8c is lower than that of [Ir(piq)$_2$(DBDIP)](PF$_6$).

The quantum yield Φ ([Ru(bpy)$_3$]$^{2+}$, 0.81, methanol) [29] was calculated based on the following Eq. [30]:

$$\Phi_{sample} = \Phi_{Ref} \times \left(K_{sample}/K_{Ref}\right) \times \left(F_{Ref}/F_{sample}\right).$$

K is the slope, F is calibration factor of the absorbance, $F = 1–10^{-OD}$ (OD is the absorbance of the photosensitizer at the light source wavelength). The quantum yield Φ was calculated to be 0.44, 0.55 and 0.61 for 8a, 8b and 8c, respectively. These complexes show moderate quantum yield. Therefore, the complexes exhibit moderate photocytotoxicity.

We also measured the generation of superoxide anion ($O_2^{\bullet-}$) using dihydrorhodamine 123 (DHR123) as a probe. The fluorescence intensity increased by 22.04, 28.18 and 19.75 times for 8a, 8b and 8c (Fig. 1c and d), which confirmed that 8a, 8b and 8c may produce $O_2^{\bullet-}$. The quantum yield Φ was measured to be 0.012 for 8a, 0.036 for 8b and 0.024 for 8c ([Ru(bpy)$_3$]$^{2+}$ in PBS, 0.042) [31]. As a result, upon light irradiation, 8a, 8b and 8c not only generate $^1O_2$, but also produce $O_2^{\bullet-}$, they may be used as type I and II photosensitizer in photodynamic therapy.

The cytotoxic activity of 8a, 8b and 8c on B16 and A549 cells can be explained according to the energy gap (ΔE) between HOMO and LUMO orbitals. Generally, the low ΔE value corresponds to a high cytotoxicity. As depicted in Fig. 1e, in the LUMO orbitals, the electronic clouds distribute in the main ligand DMHBT, while the electronic cloud focus on the ancillary ligands in the HOMO orbitals, the ΔE values for 8a, 8b and 8c are 2.5565, 2.4545, 2.2983 eV, hence, the ΔE values follow the sequence of 8a > 8b > 8c, furthermore, the energy gaps between S_1 and T_1 (Fig. 1f) are the same order as the ΔE values, which indicates that the cytotoxicity follows the order of 8a < 8b < 8c, this is line with the cytotoxicity obtained from MTT experiments.

3.3. Cellular uptake studies

The iridium(III) metal complexes emit green fluorescence, and we

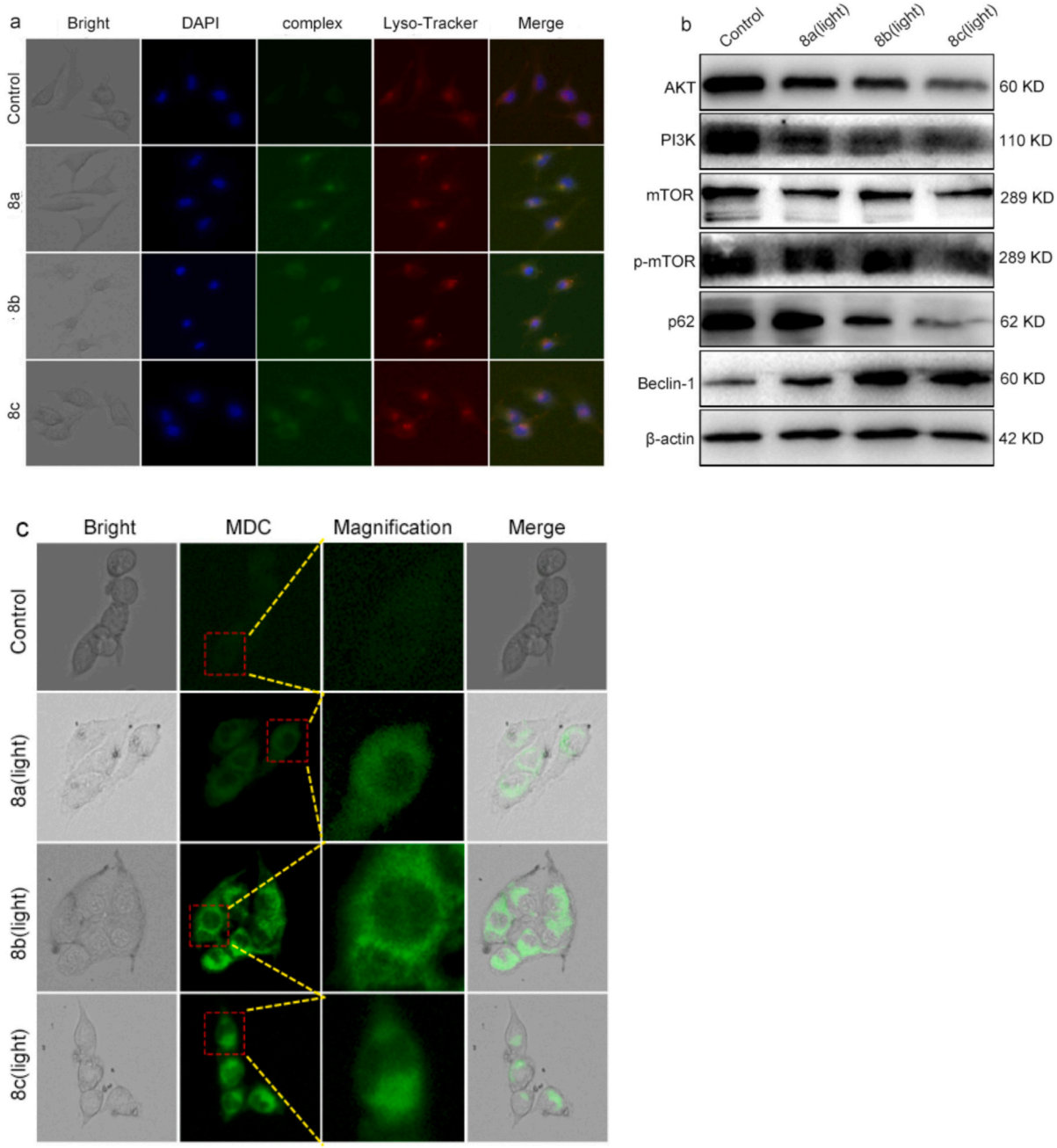

Fig. 5. (a) Co-location of 8a, 8b and 8c in the lysosomes after the treatment of B16 cells for 4 h, (b) the proteins expression induced by a treatment of B16 cells with IC_{50} concentration of 8a(light), 8b(light) and 8c(light) for 24 h, (c) autophagy assay of B16 cells treated with 2 × IC_{50} concentration of 8a(light), 8b(light) and 8c (light) for 8 h.

utilized this property to observe the cellular uptake. The cell nuclei were dyed with DAPI, after the treatment of B16 cells with 2 × IC_{50} concentration of 8a, 8b and 8c for 20 h, we observed the green fluorescence in the cells. The overlap of green fluorescence with the blue fluorescence obtained from DAPI-stained cell nuclei indicated that 8a, 8b and 8c were able to enter the cells and accumulate in the cell nuclei (Fig. S13, SI).

3.4. Co-localization at the lysosome, mitochondria, ROS and Ca^{2+} content detection

The mitochondrial pathway is one of the most important mechanisms that cause apoptosis to occur, and ROS production is inextricably linked to mitochondria. To determine the distribution of 8a, 8b and 8c inside the living cells, MitoTracker dyes as fluorescence probe was used to determine whether the complexes locate at the mitochondria. As depicted in Fig. 2a, the overlap of the fluorescence from the mitochondria (red) and the green fluorescence emitted by the complexes affirmed that 8a, 8b and 8c distributed in the mitochondria.

Mitochondria are the core of energy metabolism and the hub of calcium (Ca^{2+}) signaling, although Ca^{2+} is a positive effector of energy production, overloaded Ca^{2+} leads to mitochondrial dysfunction and thus induces cell death [32]. Further studies have confirmed that Ca^{2+} endocytosis generates ROS, and overloaded Ca^{2+} generates excess ROS which in turn causes the mitochondrial membrane permeability transition pore (MPTP) to remain open and the mitochondrial membrane potential to decrease, thereby causing mitochondrial damage and ultimately inducing the onset of apoptosis [33,34]. As observed from Fig. 2b, after B16 cells were treated with 8a, 8b, 8c and irradiated for 30

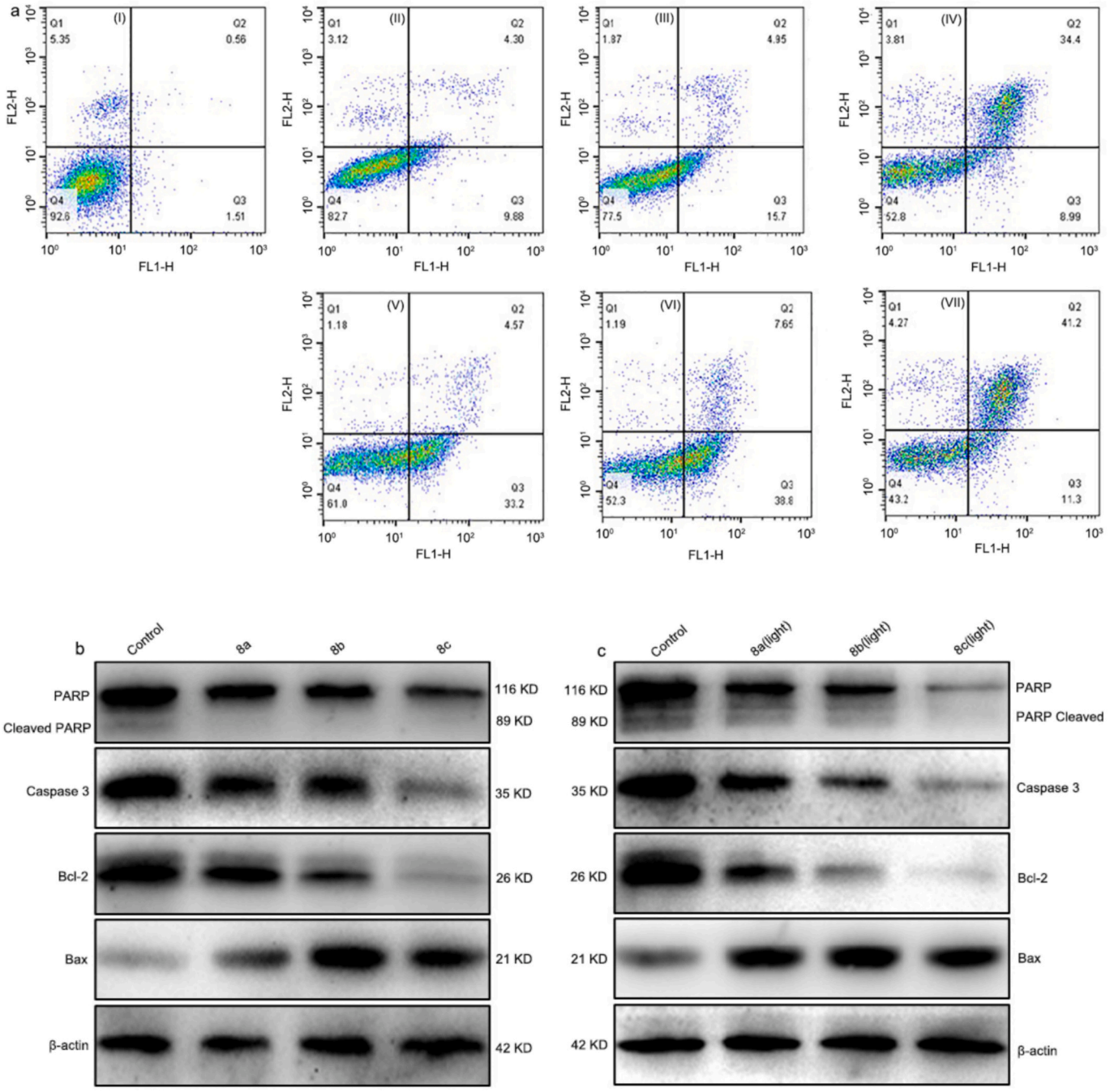

Fig. 6. (a) Apoptosis assay of B16 cells (I) treated with IC_{50} concentration of 8a (II), 8b (III), 8c (IV), 8a(light, V), 8b(light, VI) and 8c(light, VII) for 24 h, (b and c) the expression of apoptotic-related proteins in the dark or light irradiation.

min (LED lamp, 460 nm, 7.03 J/cm^2), the intracellular Ca^{2+} concentration increased, which was manifested by the significantly enhanced green fluorescence in the drug group, we observed an enhancement of the fluorescence in 8a, 8b and 8c-treated groups by 2.02, 1.55 and 1.66 times than that in the control, respectively. Next, we examined the ROS concentration (2′,7′-dichlorodihydro-fluorescein diacetate (DCFH-DA) as fluorescence probe). To eliminate the impact of the green fluorescence emitted by the complexes, the complexes were used as references. Under normal conditions, mitochondria produce appropriate amounts of reactive oxygen species (ROS) as second messengers to regulate the physiological processes, when ROS content continues to increase beyond the intracellular antioxidant system, the high ROS level leads to mitochondrial damage, autophagy, and apoptosis [35–38]. As shown in Fig. 2c, in the dark, 8a, 8b and 8c caused a slight change in the green fluorescence intensity. However, upon light irradiation, the green fluorescence increased by 30.6 times for ROSUP (positive), 176.3 times for 8a(light), 211.9 times for 8b(light) and 12.3 times for 8c(light), indicating that 8a, 8b and 8c can efficiently elevate the intracellular ROS levels upon irradiation.

To further confirm the kinds of ROS, we used dihydroethidium (DHE) as probe to examine the superoxide anion, See from Fig. 2d, the red fluorescence intensity elevated by 2.3 times for 8a(light), 2.4 times for 8b(light) and 2.7 times for 8c(light) in comparison to the control. The results suggest an ability of 8a, 8b, 8c to enhance superoxide anion. Additionally, we also examined the hydroxyl free radical content with hydroxyphenyl fluorescein (HPF) as a fluorescence probe. The green

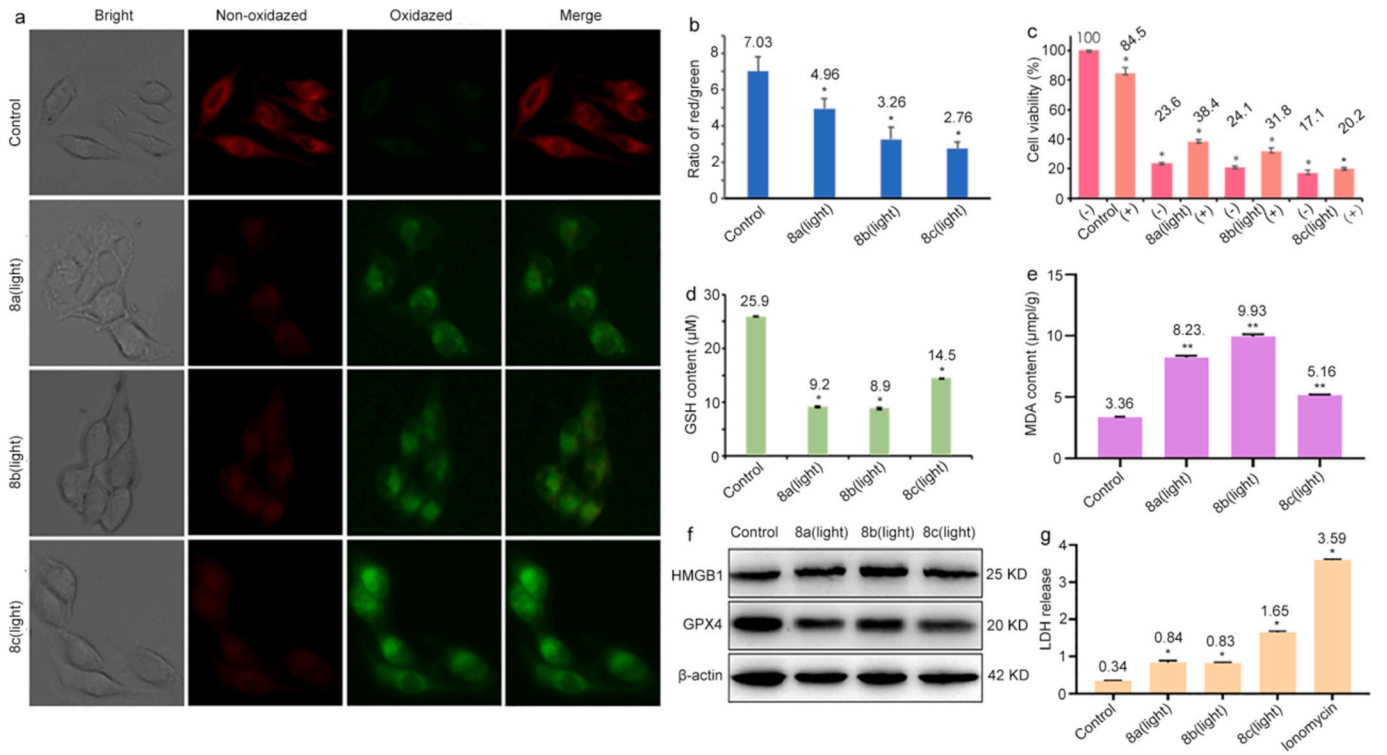

Fig. 7. (a, b) C11-BODIPY581/591 was used as a fluorescence dye to determine the red and green fluorescence, (c) cell viability assay in the presence of Fer-1, (d) GSH content, (e) MDA content, (f) release of LDH after B16 cells were incubated with IC_{50} concentrations of 8a, 8b and 8c for 24 h upon light irradiation.

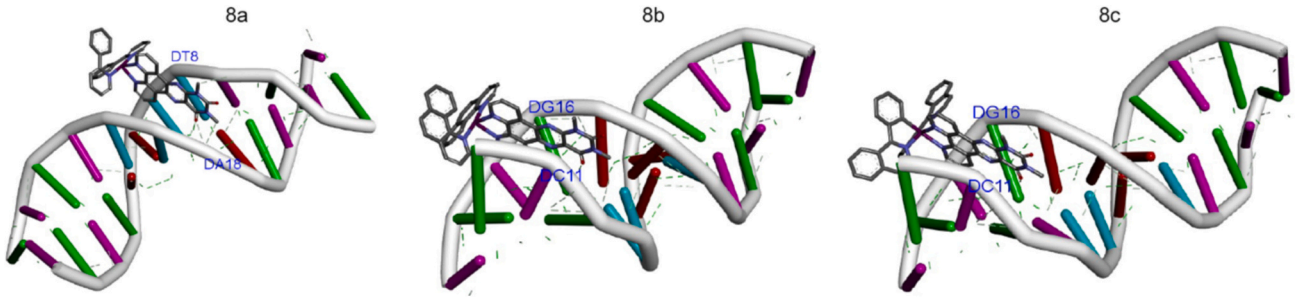

Fig. 8. Molecular docking studies of 8a, 8b and 8c with PDB ID: 1BNA.

fluorescence intensity increased by 2.44, 2.67 and 2.76 times for 8a (light), 8b(light) and 8c(light) in comparison to the control (Fig. 2e), indicating that 8a, 8b and 8c can elevate the intracellular hydroxyl free radical content upon light irradiation. Taken together, we conclude that 8a, 8b and 8c can generate $O_2^{\bullet-}$ and ·OH upon light irradiation.

The complexes act on the mitochondria and cause an increase of ROS, which will trigger an open of mitochondrial permeability transition pore (MPTP). To prove the envision, we applied calcein AM as a probe to examine MPTP. Calcein AM emits green fluorescence, after MPTP opens, $CoCl_2$ binds with calcein AM to quench the green fluorescence, which was confirmed by the significant reduction of green fluorescence in the positive, 8a(light), 8b(light) and 8c(light)-treated groups in comparison to the control (Fig. 2f), suggesting that 8a (light), 8b(light) and 8c(light) were able to induce the sustained opening of MPTP.

The opening of MPTP will lead to the decrease of mitochondrial membrane potential (MMP). To affirm this hypothesis, JC-1 (5,5′,6,6′-tetrachloro-1,1′,3,3′-tetraethylbenzenecarboxamidinylcarbocyanine iodide) was used to examine the change of mitochondrial membrane potential (MMP). It is well known that JC-1 is freely transmitting through the cell, when the mitochondria is depolarized, the JC-1 polymer is cleaved into monomers, and the fluorescence changes from red to green [39]. As shown in Fig. 2g, there was a significant decrease in red fluorescence in the 8a(light), 8b(light) and 8c(light) groups compared to the control. On the contrary, the green fluorescence was significantly enhanced, which can be further illustrated by the red/green ratio. The ratio of red/green fluorescence decreased (Fig. 2h), which affirmed that 8a(light), 8b(light) and 8c(light) can trigger a decline of MMP.

3.5. Cell cycle distribution

Cell proliferation is an important way to maintain biological growth and development, but it is also a major mechanism for cancer development [40–42]. The infinite proliferation of tumor cells makes cancer an extremely destructive and incurable disease, therefore, hindering the development of the cell cycle has become a main tactics in the cancer therapy, inhibiting the proliferation of tumor cells stops the development of malignant tumors. In this regard, we carried out experiments to explore the effects of 8a, 8b and 8c on the cell cycle of B16 with or without irradiation. Comparing with the blank group (a), the distribution of B16 cells in G0/G1 phase after the action of 8a (b), 8b (c) and 8c (d) was slightly increased by 4.00, 6.91 and 2.01 %. However, upon

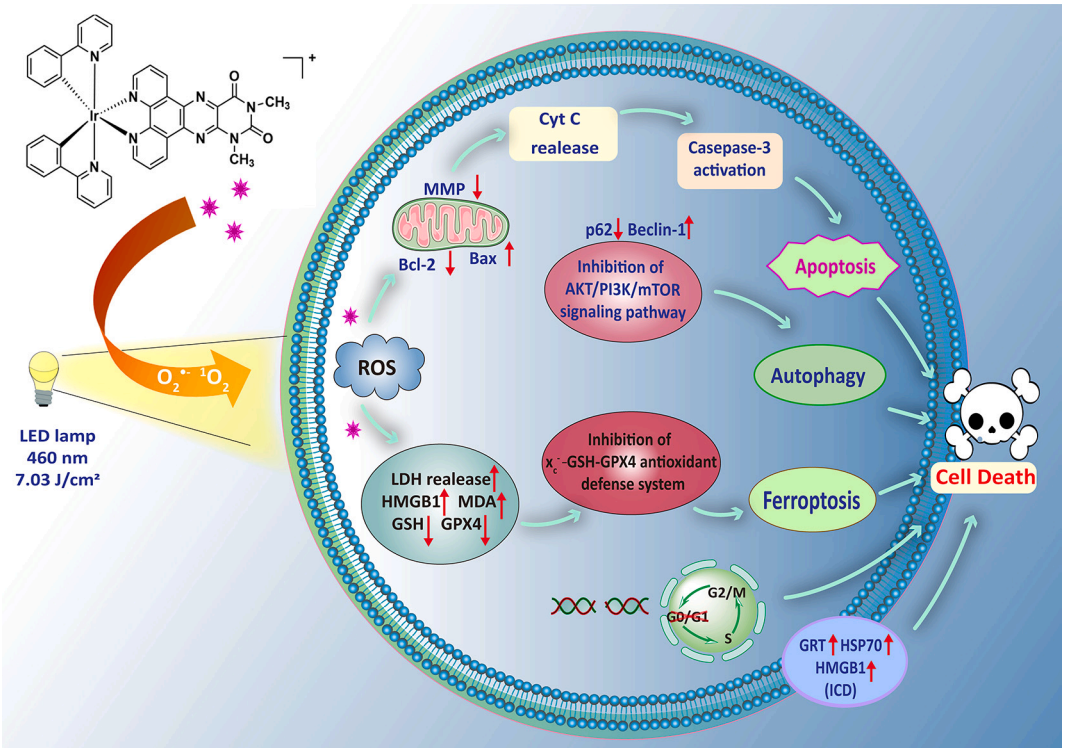

Fig. 9. Mechanism of the complexes inducting cell death.

irradiation, in comparison to the control, the distribution of cells in G0/G1 phase increased by 9.98, 10.81 and 11.23 % for 8a(light, e), 8b(light, f) and 8c(light, g) (Fig. 3). Obviously, upon irradiation, the complexes show higher efficiency on preventing cell proliferation at the G0/G1 phase than those without irradiation.

3.6. Cell death studies

3.6.1. Cellular immunogenicity assay

Immunogenic cell death (ICD) is a form of regulatory cell death that activates tumor-specific immune responses. In certain photodynamic therapy and radiotherapy treatments, signals released by inducing apoptosis in tumor cells that can serve as an immune response are damage-associated molecular patterns (DAMPs) [43], which can release calreticulin protein (CRT), heat shock proteins (HSP) and high mobility group box-1 (HMGB1). Therefore, inducing tumor cells to undergo immunogenic cell death to release damage-associated molecular patterns has become a key manner in antitumor therapy [44]. As depicted in Fig. 4a-c, upon irradiation, the green fluorescence increases, indicating interaction of 8a(light), 8b(light) and 8c(light) on B16 cells causes an enhancement of CRT (a), HSP70 (b) and HMGB1 (c) proteins. The results demonstrate that 8a, 8b and 8c can induce immunogenic cell death in B16 cells upon irradiation.

3.6.2. Autophagy studies

Autophagy is an important strategy in tumor therapy, which is crucial to maintain cellular homeostasis in response to different forms of stress in vivo and ex vivo. While macroautophagy is a lysosome-dependent degradation pathway involving the degradation of cytoplasmic proteins and organelles [45,46]. Lysosomes contain a variety of hydrolytic enzymes, which are involved in a variety of biochemical functions, and can break down biomolecules by releasing hydrolytic enzymes to remove digested remnants in the organelles while supplying energy to the cells. Hence, we firstly investigated whether the complexes enter the lysosomes. After B16 cells were subjected to 8a (8.2 μM), 8b (6.5 μM) and 8c (1.1 μM) for 4 h, the green fluorescence emitted by 8a, 8b and 8c was found to be able to overlap with the red (lysosome), indicating that 8a, 8b and 8c were able to enter the lysosome (Fig. 5a). We further explored the effect of 8a, 8b and 8c on the autophagy upon irradiation (LED lamp, 460 nm, 7.03 J/cm^2). AKT/PI3K/mTOR signaling pathway is the main pathway that initiates and mediates the occurrence of autophagy in cells, when this signaling pathway is activated, the autophagy is inhibited, inversely, when this pathway is inhibited, the expression of AKT, PI3K, and mTOR proteins decreases, and the autophagy will be activated [47]. It has been demonstrated that inhibition of melanoma growth can be achieved by inhibiting this signaling pathway [48]. The polyubiquitin-binding protein p62 binds the autophagy marker light chain 3 (LC3) for transport to autophagosomes, where it is degraded by autophagy [49]. Beclin-1 is essential for the formation and maturation of autophagosomes [50]. 8a(light), 8b (light) and 8c(light) reduced AKT, PI3K, mTOR, p-mTOR, p62 expression and upregulated the expression of Beclin-1 (Fig. 5b), which indicated that 8a(light), 8b(light) and 8c(light) can induce cellular autophagy by inhibiting the AKT/PI3K/mTOR signaling pathway. Additionally, we also investigated the autophagy using monodansylcadaverine (MDC) as green fluorescence probe. As depicted in Fig. 5c, treatment of B16 cells with 2 × IC_{50} concentration of 8a(light), 8b(light) and 8c(light) for 8 h, the autophagic vesicles were uncovered, indicating that 8a, 8b and 8c can cause autophagy upon light irradiation.

3.6.3. Apoptosis and mechanism studies

Apoptosis is the autonomous death of cells under gene regulation, which is a way for the body to remove senescent and damaged cells. Cancer is a disease of cell-autonomous proliferation that fails to respond to appropriate stimuli to evade apoptosis, resulting in unlimited proliferation of cancer cells [51]. To explore the apoptotic efficiency of the complexes, Annexin V/PI were used as a double staining probe. In the dark conditions, 8a (II), 8b (III) and 8c (IV) cause an early apoptosis with an increase of 8.37 %, 14.19 % and 7.48 %, respectively. However, upon irradiation, 8a(light) (V), 8b(light) (VI) and 8c(light) (VII) increased by 31.7 %, 37.3 % and 9.8 % in the cells at the early apoptosis (Fig. 6a). These results revealed that 8a, 8b and 8c can cause apoptosis with or not

irradiation, moreover, 8a, 8b and 8c show higher apoptotic efficiency upon irradiation than those in the dark. The above results also demonstrate that 8a and 8b may be as effective photosensitizers to cause apoptosis.

Apoptosis includes intrinsic and extrinsic pathways, which is basically characterized by the fact that pro-apoptotic proteins (e.g., Bax, Bak) and anti-apoptotic proteins (Bcl-2) of the Bcl-2 family promote the release of cytochrome *c* from mitochondria, which activates the downstream cascade reaction of caspases to cleave a variety of proteins, ultimately leading to the occurrence of apoptosis. Activation of caspase 3 and cleavage of PARP proteins, which are hallmarks of apoptosis, are used to identify the cell death pathways involved [52]. The expression levels of apoptotic proteins were examined by western blot, and the results were shown in Fig. 6b and c, we discovered that 8a, 8b and 8c can effectively downregulate the expression of PARP, caspase 3 and Bcl-2, upregulate the expression of Bax upon light irradiation or not, furthermore, 8a(light), 8b(light) and 8c(light) cause higher efficiency on the protein expression than 8a, 8b and 8c.

3.6.4. Ferroptosis studies

Among the many different forms of regulated cell death, ferroptosis is a ROS-dependent regulated cellular necrosis, which is mainly caused by intracellular oxidative membrane damage due to iron accumulation and lipid peroxidation. Imbalance in intracellular redox regulation, ROS overload, and massive production of lipid peroxides play an important role in promoting ferroptosis [53–55]. To study lipid peroxidation caused by 8a(light), 8b(light) and 8c(light), 4,4-difluoro-5-methyl-4-bora-3a,4a-diaza-s-indacene-3-dodecanoic acid (C11-BODIPY$^{581/591}$) was emerged as a probe [56]. Treatment of B16 cells with IC_{50} concentrations of 8a(light), 8b(light), and 8c(light) resulted in a significant decrease in the red fluorescence (non-oxidized) and an increase in the green fluorescence (oxidized) (Fig. 7a). In addition, Fig. 7b shows a decrease in the red/green fluorescence ratio. These results confirmed that 8a(light), 8b(light) and 8c(light) can cause lipid peroxidation.

The ability to enhance intracellular iron accumulation by increasing iron uptake, limiting iron efflux and decreasing intracellular iron storage promoted ferroptosis. Ferritin-1 (Fer-1), as an inhibitor for the ferroptosis, was used to examine cell survival. Fig. 7c reveals that the presence of Fer-1 was effective on increasing cell survival in the 8a(light), 8b (light) and 8c(light) groups, thus further confirming the potential of light-activated 8a, 8b and 8c to induce ferroptosis.

X_c^--system-glutathione (GSH)-glutathione peroxidase 4 (GPX4) is the major antioxidant defense mechanism against the onset of ferroptosis, GSH is an essential cofactor for the proper function of GPX4, and increased GSH expression inhibits ferroptosis. In addition, ferroptosis can be caused by activation of high mobility group protein 1 (HMGB1), which acts as both a damage-associated molecule and a link between ferroptosis and pyroptosis. Fig. 7d shows that 8a(light), 8b(light) and 8c (light) were able to significantly reduce the GSH content, suggesting that the three complexes were effective on reducing the content of GSH upon light exposure. Additionally, we uncovered that 8a(light), 8b(light) and 8c(light) increased the content of malondialdehyde (MDA) (a product of lipid peroxidation) (Fig. 7e). Fig. 7f shows that the three complexes were able to up-regulate HMGB1 and inhibit the expression of GPX4 after light activation, enhanced the release of LDH (Fig. 7 g). Taken together, we concluded that 8a(light), 8b(light) and 8c(light) were able to inhibit the x_c^--system-GSH-GPX4 defense mechanism and induce ferroptosis.

3.7. DNA-binding and molecular docking studies

The complexes enter cancer cells and accumulate in the cell nuclei, which stimulates us to consider whether DNA become a drug target. Hence, we investigate the DNA-binding of 8a, 8b and 8c with calf thymus (CT-DNA). The absorbance of 8a at 269 nm, 8b at 265 nm and 8c at 294 nm gradually decreased with an increment of DNA amount with a hypochmism of 13.6 %, 15.2 % and 15.9 % for 8a, 8b and 8c (Fig. S14a, SI). The DNA-binding affinities (Fig. S14b, SI) were measured to be 1.74 ($\pm$ 0.42) $\times$ 10^5 for 8a, 1.80 ($\pm$ 0.51) $\times$ 10^5 for 8b, 2.47 ($\pm$ 0.60) $\times$ 10^5 for 8c. The DNA-binding affinities are comparable with Ru(II) complex Δ-$[Ru(bpy)_2(dmppd)]^{2+}$ (3.1 $\pm$ 0.3) $\times$ 10^5 M^{-1} [18] and $[Co(bpy)_2(DMHBT)]^{3+}$ (6.3 $\pm$ 0.1) $\times$ 10^5 M^{-1} [57]. Therefore, the complexes exhibit high DNA-binding ability. The DNA-binding affinities follow the sequence of 8c > 8b > 8a, this is well line with those of cytotoxicity. The binding site and binding energy with double strand DNA (PDB ID: 1BNA) were calculated through molecular docking (Autodock 4.2). 8a, 8b and 8c interact with DNA through intercalation at the minor groove accompanied by hydrogen bond of DA18:H3 for 8a, DG16:H22 for 8b and 8c (Fig. 8), respectively. The binding energy of 8a, 8b, 8c with DNA is −36.4, −37.2 and − 40.5 KJ·mol^{-1}. The results from the binding energy show that DNA-binding affinity is 8a < 8b < 8c, this is consistent with the sequence from electronic absorption titration. Consequently, we conclude that the complexes target the DNA and induce cancer cell demise.

4. Conclusions

Three new iridium(III) metal complexes with DMHBT as ligand were synthesized. Single state oxygen and superoxide anion assays showed that 8a, 8b and 8c can increase $^1O_2$ and $O_2^{\bullet-}$ as photosensitizers for the treatment of cancer in photodynamic therapy. In vitro cytotoxicity experiments revealed that 8a, 8b and 8c exhibited moderate or low cytotoxicity against various tumor cell lines, whereas the in vitro toxicity of the complexes was greatly improved upon light irradiation, with the strong ability to kill B16 cells. The cellular uptake demonstrated that the complexes enter the cells and accumulate in the cell nuclei.Co-localization experiments revealed that the complexes were able to localize at the mitochondria. Since apoptosis via the intrinsic pathway is mediated by oxidatively damaged mitochondria, we found that the complexes led to a massive inward flow of Ca^{2+} and a great enhancement of ROS, which in turn led to the sustained opening of the MPTP and the decrease of MMP, resulting in mitochondrial dysfunction and inducing B16 cells to undergo apoptosis. The mechanism studies found that 8a(light), 8b(light) and 8c(light) activated Bcl-2 family proteins and caused caspase cascade reaction to induce apoptosis. The complexes can arrest the cell cycle at the G0/G1 phase, blocking DNA synthesis and contributing to cell death. We also found that 8a(light), 8b(light) and 8c (light) inhibit the AKT/PI3K/mTOR signaling pathway, down-regulate p62 and promote the expression of Beclin-1, which induced cells to undergo autophagy. In addition, 8a(light), 8b(light) and 8c(light) caused a dramatic increase in ROS levels in B16 cells. Further experiments revealed that overloaded ROS reacted with polyunsaturated fatty acids to initiate lipid peroxidation, inhibited the x_c^--system-glutathione (GSH)-glutathione peroxidase 4 (GPX4) antioxidant defense system, and up-regulated the expression of the damage-associated molecule HMGB1 to cause ferroptosis. It also promotes the release of CRT and HSP70, which activates tumor-specific immune responses to trigger immunogenic cell death. In summary, 8a, 8b and 8c as photosensitizers target the DNA and induce cell death via the following five pathways: (I) ROS-mediated mitochondrial dysfunction apoptosis; (II) blocking the cell cycle at G0/G1 phase and inhibiting cell proliferation; (III) inducing cellular autophagy; (IV) causing ferroptosis and (V) immunogenic cell death (Fig. 9). The present work contributes to the further understanding the anticancer mechanism and provides an help for the design and synthesis of photocytotoxic candidates for the treatment of B16 tumors.

Author statement

We state that the manuscript has been finished by all authors listed in the manuscript. The all data are original and real. We agree to be accountable for all aspects of the work to ensure that questions related to the accuracy or integrity of any part of the work are appropriately investigated and resolved.

All authors have read the manuscript and approved the manuscript to be submitted to JIB.

CRediT authorship contribution statement

Yajie Niu: Methodology, Investigation. **Shuanghui Tang:** Software, Data curation. **Jiongbang Li:** Formal analysis. **Chunxia Huang:** Investigation. **Yan Yang:** Writing – original draft, Conceptualization. **Lin Zhou:** Software, Formal analysis. **Yunjun Liu:** Supervision, Funding acquisition, Conceptualization. **Xiandong Zeng:** Writing – review & editing, Project administration, Investigation.

Declaration of competing interest

Authors declare no competing interests exist.

Acknowledgments

We are grateful for National Natural Science Foundation of China (No 21877018).

Appendix A. Supplementary data

Materials and methods, cellular uptake assay, detection of intracellular localization and mitochondrial membrane potential, apoptosis detection by flow cytometry, Cell cycle research, autophagy assay, Ca^{2+} content detection, reactive oxygen (ROS) content measurement, immunochromatography, MDA content determination, determination of intracellular glutathione (GSH) content, lipid-water partition coefficient determination, protein extraction in the supporting information. Supplementary data to this article can be found online at [https://doi.org/10.1016/j.jinorgbio.2024.112808].

Data availability

Data will be made available on request.

References

[1] F. Tas, Metastatic behavior in melanoma: timing, pattern, survival, and influencing factors, J. Oncol. 2012 (2012) 647684.
[2] B. Li, X.L. Zhang, Y. Lu, L.Y. Zhao, Y.X. Guo, S.S. Guo, Q.Z. Kang, J.J. Liu, L.P. Dai, L.G. Zhang, D.D. Fan, Z.Y. Ji, Protein 4.1R affects photodynamic therapy for B16 melanoma by regulating the transport of 5-aminolevulinic acid, Exp. Cell Res. 399 (2021) 112465.
[3] G. Canti, D. Lattuada, S. Morelli, A. Nicolin, R. Cubeddu, P. Taroni, G. Valentini, Efficacy of photodynamic therapy against doxorubicin-resistant murine tumors, Cancer Lett. 93 (1995) 255–259.
[4] M.P.D. Grande, A.M. Miyake, M.K. Nagamine, J.V.P. Leite, L.L.M. Fonseca, C. O. Massoco, M.L.Z. Dagli, Methylene blue and photodynamic therapy for melanomas: inducing different rates of cell death (necrosis and apoptosis) in B16-F10 melanoma cells according to methylene blue concentration and energy dose, Photodiagn. Photodyn. Ther. 37 (2022) 102635.
[5] T.C. Pham, V.N. Nguyen, Y. Choi, S. Lee, J. Yoon, Recent strategies to develop innovative photosensitizers for enhanced photodynamic therapy, Chem. Rev. 121 (2021) 13454–13619.
[6] W. Fan, P. Huang, X. Chen, Overcoming the achilles heel of photodynamic therapy, Chem. Soc. Rev. 45 (2016) 6488–6519.
[7] S. Ye, J. Rao, S. Qiu, J. Zhao, H. He, Z. Yan, T. Yang, Y. Deng, H. Ke, H. Yang, Y. Zhao, Z. Guo, H. Chen, Rational design of conjugated photosensitizers with controllable photoconversion for dually cooperative phototherapy, Adv. Mater. 30 (2018) 1801216.
[8] N. Clemente, I. Miletto, E. Gianotti, M. Sabbatini, M. Invernizzi, L. Marchese, U. Dianzani, F. Renò, Verteporfin-loaded mesoporous silica nanoparticles' topical applications inhibit mouse melanoma lymphangiogenesis and micrometastasis in vivo, Int. J. Mol. Sci. 22 (2021) 13443.
[9] J. Li, J.H. Li, Y.J. Pu, S. Li, W.X. Gao, B. He, PDT-enhanced ferroptosis by a polymer nanoparticle with pH-activated singlet oxygen generation and superb biocompatibility for cancer therapy, Biomacromolecules 22 (2021) 1167–1176.
[10] R. Alzeibak, T.A. Mishchenko, N.Y. Shilyagina, I.V. Balalaeva, M.V. Vedunova, D. V. Krysko, Targeting immunogenic cancer cell death by photodynamic therapy: past, present and future, J. Immunother. Cancer 9 (2021) e001926.
[11] S. Tian, Q.Y. Nie, H.M. Chen, L.J. Liang, H.Y. Hu, S.H. Tang, J.W. Yang, Y.J. Liu, H. Yin, Synthesis, characterization and irradiation enhances anticancer activity of liposome-loaded iridium(III) complexes, J. Inorg. Biochem. 256 (2024) 112549.
[12] T. Feng, Z.X. Tang, J. Karges, J. Sun, K. Xiong, C.Z. Jin, Y. Chen, G. Gasser, L.N. Ji, H. Chao, An iridium(III)-based photosensitizer disrupting the mitochondrial respiratory chain induces ferritinophagy-mediated immunogenic cell death, Chem. Sci. 15 (2024) 6752–6762.
[13] J. Kasparkova, A. Hernández-García, H. Kostrhunova, M. Goicuría, V. Novohradsky, D. Bautista, L. Markova, M.D. Santana, V. Brabec, J. Ruiz, Novel 2-(5-Arylthiophen-2-yl)-benzoazole cyclometalated iridium(III) dppz complexes exhibit selective phototoxicity in cancer cells by lysosomal damage and oncosis, J. Med. Chem. 67 (2024) 691–708.
[14] J. Karges, Clinical development of metal complexes as photosensitizers for photodynamic therapy of cancer, Angew. Chem. Int. Ed. 61 (2022) e202112236.
[15] W.Y. Zhang, Q.Y. Yi, Y.J. Wang, F. Du, M. He, B. Tang, D. Wan, Y.J. Liu, H. L. Huang, Photoinduced anticancer activity studies of iridium(III) complexes targeting mitochondria and tubules, Eur. J. Med. Chem. 151 (2018) 568–584.
[16] G.C. Li, J. Chen, Y.F. Xie, Y. Yang, Y.J. Niu, X.L. Chen, X.D. Zeng, L. Zhou, Y.J. Liu, White light increases anticancer effectiveness of iridium(III) complexes toward lung cancer A549 cells, J. Inorg. Biochem. 259 (2024) 112652.
[17] W. Li, C. Shi, X. Wu, Y. Zhang, H. Liu, X. Wang, C. Huang, L. Liang, Y. Liu, Light activation of iridium(III) complexes driving ROS production and DNA damage enhances anticancer activity in A549 cells, J. Inorg. Biochem. 236 (2022) 111977.
[18] F. Gao, H. Chao, F. Zhou, L.C. Xu, K.C. Zheng, L.N. Ji, Synthesis, characterization, and DNA-binding properties of the chiral ruthenium(II) complexes Δ- and Λ-[Ru(bpy)$_2$(dmppd)]$^{2+}$ (dmppd = 10,12-dimethylpteridino[6,7-f][1,10]phenanthroline-11,13(10H,12H)-dione; bpy=2,2′-bipyridine), Helv. Chim. Acta 90 (2007) 36–51.
[19] S. Sprouse, K.A. King, P.J. Spellane, R.J. Watts, Photophysical effects of metal-carbon bonds in ortho-metalated complexes of Ir(III) and Rh(III), J. Am. Chem. Soc. 106 (1984) 6647–6653.
[20] T. Mosmann, Rapid colorimetric assay for cellular growth and survival: application to proliferation and cytotoxicity assays, J. Immunol. Methods 65 (1983) 55–63.
[21] E. Baka, J.E.A. Comer, K. Takács-Novák, Study of equilibrium solubility measurement by saturation shake-flask method using hydrochlorothiazide as model compound, J. Pharm. Biomed. Anal. 46 (2008) 335–341.
[22] P.Y. Zhang, H.Y. Huang, S. Banerjee, G.J. Clarkson, C. Ge, C. Imberti, P.J. Sadler, Nucleus-targeted organoiridium–albumin conjugate for photodynamic cancer therapy, Angew. Chem. Int. Ed. 58 (2019) 2350–2354.
[23] P.S. Maharjan, H.K. Bhattarai, Singlet oxygen, photodynamic therapy, and mechanisms of cancer cell death, J. Oncol. 2022 (2022) 7211485.
[24] P. Agostinis, K. Berg, K.A. Cengel, T.H. Foster, A.W. Girotti, S.O. Gollnick, S. M. Hahn, M.R. Hamblin, A. Juzeniene, D. Kessel, M. Korbelik, J. Moan, P. Mroz, D. Nowis, J. Piette, B.C. Wilson, J. Golab, Photodynamic therapy of cancer: an update, CA Cancer J. Clin. 61 (2011) 250–281.
[25] S. Kwiatkowski, B. Knap, D. Przystupski, J. Saczko, E. Kędzierska, K. Knap-Czop, J. Kotlińska, O. Michel, K. Kotowski, J. Kulbacka, Photodynamic therapy-mechanisms, photosensitizers and combinations, Biomed. Pharmacother. 106 (2018) 1098–1107.
[26] Y.J. Hou, X.X. Yang, R.Q. Liu, D. Zhao, C.X. Guo, A.C. Zhu, M.N. Wen, Z. Liu, G. F. Qu, H.X. Meng, Pathological mechanism of photodynamic therapy and photothermal therapy based on nanoparticles, Int. J. Nanomedicine 15 (2020) 6827–6838.
[27] J. Gustalik, D. Aebisher, D. Bartusik-Aebisher, Photodynamic therapy in breast cancer treatment, J. Appl. Biomed. 20 (2022) 98–105.
[28] L. Zhou, J.B. Li, J. Chen, X. Yao, X.D. Zeng, Y. Wang, Y.J. Liu, X.Z. Wang, Anticancer activity and mechanism studies of photoactivated iridium (III) complexes toward lung cancer A549, Dalton Trans. 53 (2024) 15176–15189.
[29] K. Bhattacharyya, P.K. Das, Quantitative aspects of all-trans-retinol singlet and triplet quenching by oxygen, Chem. Phys. Lett. 116 (1985) 326–331.
[30] L.V. Lutkus, S.S. Rickenbach, T.M. Mccormick, Singlet oxygen quantum yields determined by oxygen consumption, J. Photoch. Photobiol. A 378 (2019) 131–135.
[31] J.V. Caspar, T.J. Meyer, Photochemistry of Ru(bpy)$_3^{2+}$ solvent effect, J. Am. Soc. Chem. 105 (1983) 5583–5589.
[32] R.F. Feissner, J. Skalska, W.E. Gaum, S.S. Sheu, Crosstalk signaling between mitochondrial Ca^{2+} and ROS, Front. Biosci. 14 (2009) 1197.
[33] T.Y. Kim, R. Terentyeva, K.H. Roder, W. Li, M. Liu, I. Greener, S. Hamilton, I. Polina, K.R. Murphy, R.T. Clements, S.C.J. Dudley, G. Koren, B.R. Choi, D. Terentyev, SK channel enhancers attenuate Ca^{2+}-dependent arrhythmia in hypertrophic hearts by regulating Mito-ROS-dependent oxidation and activity of RyR, Cardiovasc. Res. 113 (2017) 343–353.
[34] C. Cui, R. Merritt, L. Fu, Z. Pan, Targeting calcium signaling in cancer therapy, Acta Pharm. Sin. B 7 (2017) 3–17.
[35] S. Antonucci, F.D. Lisa, N. Kaludercic, Mitochondrial reactive oxygen species in physiology and disease, Cell Calcium 94 (2021) 102344.
[36] H.D. Guthrie, G.R. Welch, Determination of intracellular reactive oxygen species and high mitochondrial membrane potential in Percoll-treated viable boar sperm using fluorescence-activated flow cytometry, J. Anim. Sci. 84 (2006) 2089–2100.
[37] K.C. Chuang, C.R. Chang, S.H. Chang, S.W. Huang, S.M. Chuang, Z.Y. Li, S. T. Wang, J.K. Kao, Y.J. Chen, J.J. Shieh, Imiquimod-induced ROS production disrupts the balance of mitochondrial dynamics and increases mitophagy in skin cancer cells, J. Dermatol. Sci. 98 (2020) 152–162.
[38] D.F. Zou, A.L. Zhang, J.J. Chen, Z.Q. Chen, J. Deng, G. Li, S.L. Zhang, Z. Feng, J. F. Feng, J. Yang, Designing a lysosome targeting nanomedicine for pH-triggered enhanced phototheranostics, Mater. Chem. Front. 5 (2021) 2694–2701.

[39] K. Elefantova, B. Lakatos, J. Kubickova, Z. Sulova, A. Breier, Detection of the. Mitochondrial membrane potential by the cationic dye JC-1 in L1210 cells with massive overexpression of the plasma membrane ABCB1 drug transporter, Int. J. Mol. Sci. 19 (2018) 1985.
[40] S. Diaz-Moralli, M. Tarrado-Castellarnau, A. Miranda, M. Cascante, Targeting cell cycle regulation in cancer therapy, Pharmacol. Ther. 138 (2013) 255–271.
[41] Y. Sun, Y. Liu, X.L. Ma, H. Hu, The influence of cell cycle regulation on chemotherapy, Int. J. Mol. Sci. 22 (2021) 6923.
[42] S. Ghafouri-Fard, H. Shoorei, F.T. Anamag, M. Taheri, The role of non-coding RNAs in controlling cell cycle related proteins in cancer cells, Front. Oncol. 10 (2020) 608975.
[43] A. Ahmed, S.W.G. Tait, Targeting immunogenic cell death in cancer, Mol. Oncol. 14 (2020) 2994–3006.
[44] J. Cui, H. Xu, J. Shi, K. Fang, J. Liu, F. Liu, Y. Chen, H.Y. Liang, Y. Zhang, H.Z. Piao, Carbonic anhydrase IX inhibitor S4 triggers release of DAMPs related to immunogenic cell death in glioma cells via endoplasmic reticulum stress pathway, Cell Commun. Signal 21 (2023) 167.
[45] K.R. Martin, S.L. Celano, A.R. Solitro, H. Gunaydin, M. Scott, R.C. O'Hagan, S. D. Shumway, P. Fuller, J.P. MacKeigan, A potent and selective ULK1 inhibitor suppresses autophagy and sensitizes cancer cells to nutrient stress, iSci 8 (2018) 74–84.
[46] S.S. Singh, S. Vats, A.Y. Chia, T.Z. Tan, S. Deng, M.S. Ong, F. Arfuso, C.T. Yap, B. C. Goh, G. Sethi, R.Y. Huang, H.M. Shen, R. Manjithaya, A.P. Kumar, Dual role of autophagy in hallmarks of cancer, Oncogene 37 (2018) 1142–1158.
[47] J. Zhou, Y. Jiang, H. Chen, Y.C. Wu, L. Zhang, Tanshinone I attenuates the malignant. Biological properties of ovarian cancer by inducing apoptosis and autophagy via the inactivation of PI3K/AKT/mTOR pathway, Cell Prolif. 53 (2020) e12739.
[48] J. Wang, T. Sinnberg, H. Niessner, R. Dölker, B. Sauer, W.E. Kempf, F. Meier, N. Leslie, B. Schittek, PTEN regulates IGF-1R-mediated therapy resistance in melanoma, Pigm. Cell Melanoma Res. 28 (2015) 572–589.
[49] G. Bjørkøy, T. Lamark, A. Brech, H. Outzen, M. Perander, A. Øvervatn, H. Stenmark, T. Johansen, p62/SQSTM1 forms protein aggregates degraded by autophagy and has a protective effect on huntingtin-induced cell death, J. Cell Biol. 171 (2005) 603–614.
[50] H.D. Xu, Z.H. Qin, Beclin 1, Bcl-2 and autophagy, Adv. Exp. Med. Biol. 1206 (2019) 109–126.
[51] P. Singh, B. Lim, Targeting apoptosis in cancer, Curr. Oncol. Rep. 24 (2022) 273–284.
[52] D. Bertheloot, E. Latz, B.S. Franklin, Necroptosis, pyroptosis and apoptosis: an intricate game of cell death, Cell. Mol. Immunol. 18 (2021) 1106–1121.
[53] X. Chen, J. Li, R. Kang, D.J. Klionsky, D.L. Tang, Ferroptosis: machinery and regulation, Autophagy 17 (2021) 2054–2081.
[54] F. Ursini, M. Maiorino, Lipid peroxidation and ferroptosis: the role of GSH and GPX4, Free Radic. Biol. Med. 152 (2020) 175–185.
[55] L. Rochette, G. Dogon, E. Rigal, M. Zeller, Y. Cottin, C. Vergely, Lipid peroxidation and iron metabolism: two corner stones in the homeostasis control of ferroptosis, Int. J. Mol. Sci. 24 (2023) 449.
[56] G.P.C. Drummen, L.C.M. van Liebergen, J.A.F. den Kamp, J.A. Post, C11-BODIPY581/591, an oxidation-sensitive fluorescent lipid peroxidation probe: (micro)spectroscopic characterization and validation of methodology, Free Radic. Biol. Med. 33 (2002) 473–490.
[57] K.S. Kumar, K.L. Reddy, S. Satyanarayana, Synthesis, DNA binding, DNA photocleavage and antimicrobial activity of $[co(bpy)_2DMHBT]^{3+}$, $[co(dmb)_2DMHBT]^{3+}$, and $[co(phen)_2DMHBT]^{3+}$ complexes, Spectrosc. Lett. 44 (2011) 27–37.